IN-02
88795

p.44

The Natural Flow
Wing-Design Concept

Richard M. Wood
and Steven X. S. Bauer

NASA

The Natural Flow Wing-Design Concept

Richard M. Wood
and Steven X. S. Bauer
Langley Research Center
Hampton, Virginia

Nomenclature

A	cross-sectional area, in^2
a_i	variables used to define airfoil geometry forward of maximum thickness (where $i = 0, 1, 2,$ or 3)
b	wing span, in.
C_D	drag coefficient, $Drag/q_\infty S$
$C_{D,cs}$	cross-sectional inviscid drag coefficient from EMTAC code, $\int C_{D,e}$
$C_{D,e}$	elemental inviscid drag coefficient from EMTAC code
$C_{D,I}$	inviscid drag coefficient, $\int C_{D,cs}$
$C_{D,i}$	induced drag coefficient from linear theory
$C_{D,o}$	zero-lift inviscid drag coefficient of uncambered wing from EMTAC
$C_{D,V}$	viscous drag coefficient
C_L	lift coefficient, $Lift/q_\infty S$
C_p	pressure coefficient, $(p - p_\infty)/q_\infty$
c	chord, in.
d_i	variables used to define airfoil geometry aft of maximum thickness location (where $i = 0, 1, 2,$ or 3)
F_c	camber function (varies in streamwise direction)
L/D	lift-drag ratio
l	wing length, in.
M	Mach number
p	local static pressure, lb/ft^2
p_∞	free-stream static pressure, lb/ft^2
q_∞	free-stream dynamic pressure, lb/ft^2
r	leading-edge radius, in.
S	wing reference area, ft^2
t	airfoil thickness, in.
Δt	change in wing thickness, used in wing asymmetry method, in.
Δt_s	change in cross-section wing thickness at centerline, used in wing shearing method, in.
x	streamwise direction
y	spanwise direction
z	direction normal to wing planform
α	angle of attack, deg
β	$= \sqrt{M^2 - 1}$
Λ	leading-edge sweep, deg

Subscripts:

$\mathcal{C}$	centerline
lower	wing lower surface
max	maximum
root	wing root chord
TE	trailing edge
tip	wingtip
upper	wing upper surface

Abbreviations:

A(n)	asymmetry (where $n = 20, 50,$ or 90)
B(n)	leading-edge bluntness (where $n = 1, 3,$ or 4)
EMTAC	Euler Marching Technique for Accurate Computation
LT	linear theory
N-C	near-conical wing
T(n)	airfoil thickness (where $n = 1$ or 3)
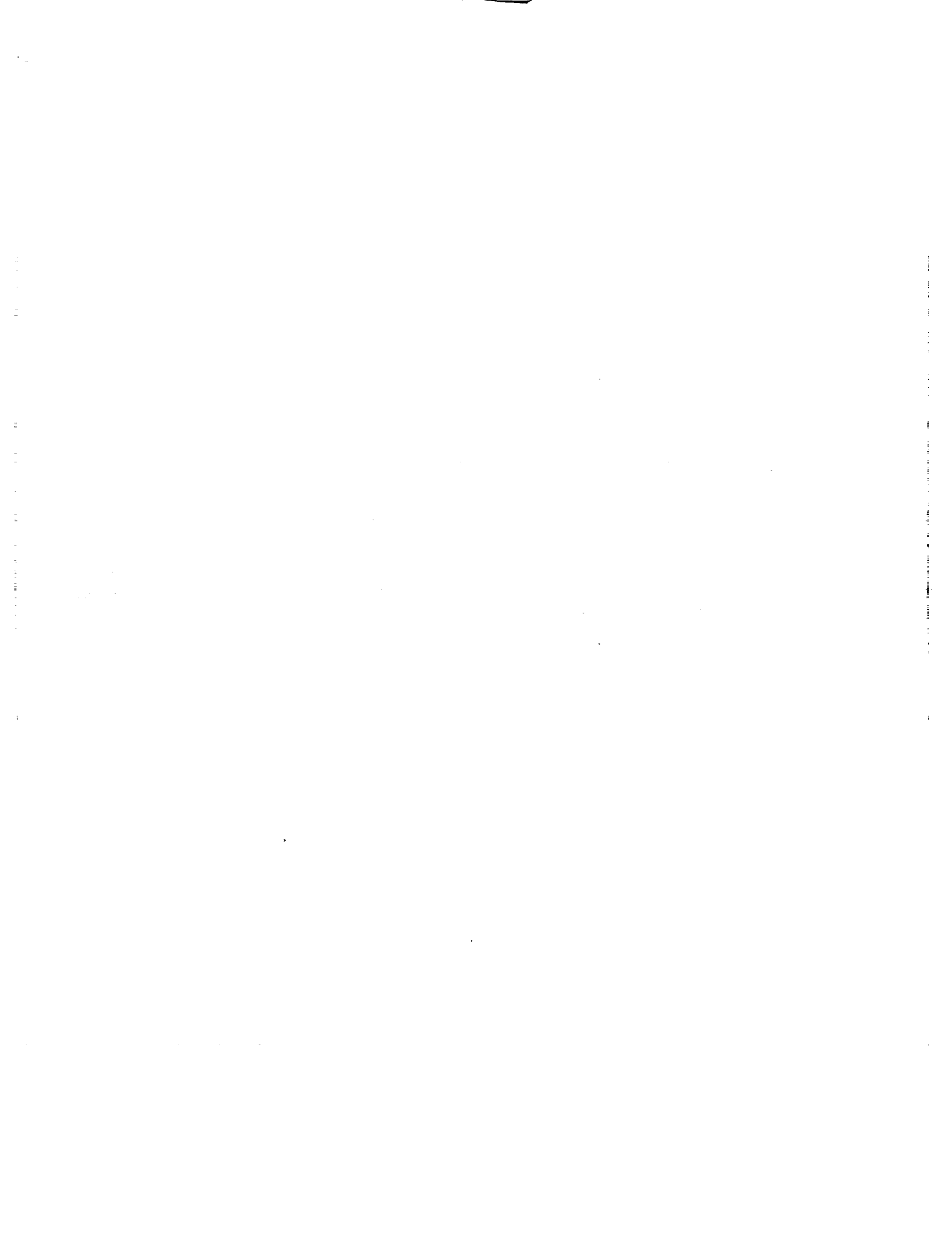
Abstract

A wing-design study has been conducted on a 65° swept leading-edge delta wing in which the wing geometry was modified to take advantage of the naturally occurring flow that forms over a slender wing in a supersonic flow field. Three-dimensional nonlinear analysis methods were used in the study which was divided into three parts—preliminary design, initial design, and final design. In the preliminary design, the wing planform, the design conditions, and the near-conical wing-design concept were derived, and a baseline standard wing (conventional airfoil distribution) and a baseline near-conical wing were chosen. During the initial analysis, a full-potential flow solver was employed to determine the aerodynamic characteristics of the baseline standard delta wing and to investigate modifications of the airfoil thickness, leading-edge radius, airfoil maximum-thickness position, and wing upper to lower surface asymmetry on the baseline near-conical wing. The final design employed an Euler solver to analyze the best wing configurations found in the initial design and to extend the study of wing asymmetry to develop a more refined wing. Benefits resulting from each modification are discussed, and a final "natural flow" wing geometry has been designed that provides an improvement in aerodynamic performance compared with that of a baseline conventional uncambered wing, linear-theory cambered wing, and near-conical wing.

Introduction

Future supersonic military or commercial aircraft will be required to have high levels of lifting efficiency at subsonic and transonic speeds as well as at supersonic speeds; however, the present wing-design philosophies that must be employed to address these multipoint design conditions vary greatly. A review of the existing wing-design philosophies for subsonic, transonic, and supersonic flight reveals several contradictions as well as several similarities. The contradictions exist mainly between the low-speed (subsonic and transonic) cruise-design philosophies (refs. 1 and 2) and the supersonic cruise-design methods (ref. 3). For subsonic and transonic designs, the tendency is to use a lower wing sweep, thick airfoils, and blunt leading edges; advanced supercritical-type airfoils are most commonly used. On the other hand, supersonic designs typically employ wings having higher sweep with thin airfoils and sharp leading edges. The supersonic wing-design tendencies are almost solely due to concerns about supersonic wave drag. Wing twist and camber at all speeds are usually provided by linear-theory-type methods.

At maneuvering conditions, both the low-speed and supersonic wing-design methods employ variable-camber devices such as leading- and trailing-edge flaps. At subsonic speeds, leading-edge flaps have been shown to be fairly successful (ref. 4); however, at

transonic and supersonic speeds, only minimal performance benefits have been achieved (ref. 5). Another drawback to variable-camber devices is the increase in complexity, wing weight, and the loss in usable wing volume. An alternate approach to the maneuver-design requirement is to develop a fixed-camber wing. In general, these wing-design studies have been fairly successful at their design lift condition, but they have suffered severe camber drag penalties at the lower lift conditions (ref. 6).

To address the need for a multipoint wing-design approach, a wing-design concept has been developed that contours the upper and lower surfaces of the three-dimensional wing independent of one another in order to take maximum advantage of the naturally occurring flow field and resultant pressure distribution. This present approach is similar to the philosophy employed in low-speed, two-dimensional (2-D) airfoil design, but it is counter to studies of traditional 3-D wing camber design. The remainder of this paper will overview the present design approach as applied to delta wings at supersonic speeds. A complete review of the iterative computational design results will be presented and discussed. This paper will summarize the results of references 7–10 in which the natural flow wing-design concept is developed and evaluated. The supporting data for this study were derived both from the application of nonlinear, inviscid, computational aerodynamic methods

(refs. 11–13) and from published force, pressure, and flow visualization data (ref. 8).

Wing-Design Philosophy

An extensive survey of the literature (ref. 8) was conducted to determine the dominant wing geometric characteristics (i.e., leading-edge-sweep and planform) and flow conditions (i.e., Mach number) that should be considered in assessing the supersonic aerodynamics of wings. The result of this effort was the identification of the delta or triangular wing planform as the most likely candidate for the development of future wing-design methods because of the extensive experimental and theoretical data base available. In addition, the empirical correlations derived for delta wings could be extended to other simple wing planforms, such as arrow and diamond wings, through the use of simple geometric and flow correlation parameters.

The conventional application of thickness to uncambered delta wings results in a wing that is conical about the wingtip. (See fig. 1.) However, experimental data (ref. 8) and theoretical analysis (ref. 11) show that the flow over a swept wing at subsonic, transonic, and supersonic speeds tends to be conical about the wing apex and not conical about the wingtip as observed for wings having small values of leading-edge sweep. The conical nature of the flow field over the delta wing upper surface produces favorable and unfavorable pressure fields, based on drag consideration (fig. 1).

For a wing at moderate-to-high lift conditions, the flow over the wing upper surface may be characterized by an expansion over the leading edge that is followed by a recompression to a more positive pressure as the flow moves inboard and aft. Through experimental observations, the location of the recompression region has been observed to lie along a ray emanating from the wing apex. If the upper surface is divided into four quadrants, defined by the intersection of the airfoil maximum half-thickness line (crest line) and the crossflow recompression line, two favorable and two unfavorable performance regions are identified. The two unfavorable regions, which contribute to the drag, are the inboard forward region (A) and the outboard aft region (C) of the wing. The inboard forward region (A) of the wing experiences a recompression of the flow prior to the airfoil crest line; this results in larger pressure coefficients acting on a forward-facing wing surface. On the other hand, the outboard aft region (C) of the wing is characterized by a rearward sloping surface that combines with the high negative pressure coefficients to produce high drag levels. The other two regions (B

and D) of the wing upper surface would have pressure fields that combine favorably with the local surface geometry to produce drag reductions. Figure 1 illustrates how a "near-conical" upper surface wing geometry could reduce the unfavorable drag regions of the wing (i.e., regions A and C) by moving the centerline airfoil crest forward and sweeping the outboard airfoil crest line aft to more closely coincide with the conical nature of the flow.

However, the flow on the lower surface of the wing behaves quite differently at positive angles of attack, therefore requiring a different type of geometry. The flow over the wing lower surface is characterized by a nearly constant compression loading. The magnitude of these compression pressures is primarily dependent upon the wing-surface streamwise slope and is not very sensitive to the curvature in the crossflow plane. Based upon these observations, the most beneficial lower surface geometry would have as large an area as possible with aft-facing slopes to take full advantage of the lower surface pressure loading.

Wing-Design Study

The wing-design study has been executed in three steps:

1. Preliminary design

2. Initial design

3. Final design

The preliminary design of step 1 phase has been documented in references 7–9 in which the wing sweep, the design conditions, and the near-conical concept were derived based upon considerations of zero-lift wave drag, wing lifting efficiency, and wing loading. The preliminary design phase considered only wing geometries that were symmetric.

Step 2 in the design process was the initial design (refs. 9 and 10) in which an iterative computational design was conducted using a full-potential-based computational method (ref. 12). The objectives of the initial design were to identify the aerodynamic performance trends associated with variations in airfoil shape (thickness, bluntness, and maximum-thickness position), the spanwise variation in airfoils, the vertical shearing of airfoils, and the redistribution of wing volume. In this phase of the design, independent variations in all geometric parameters for the wing upper and lower surfaces were investigated.

Step 3 was the final design (ref. 10) in which the wing surface was further refined through small perturbations of all geometric variables. Within this section of the design process, the primary computational tool was an Euler code (ref. 13). The figures of

merit for each of these design phases were total aero-dynamic forces and moments and wing sectional forces. Wing surface pressure distributions and detailed flow field information were also examined to assess the adequacy of the computational fluid dynamics (CFD) methodology.

Geometry

In order to implement the proposed wing-design concept in a logical fashion, a method was developed for generating wing geometry that would allow for a broad range of analytic wing surfaces to be developed from a few input parameters. Selected as the foundation of the method was the modified NACA four-digit airfoil series which can be used to define a wide range of analytic airfoil shapes. (See sketch A.) As noted in sketch A, the airfoil forward and aft sections are each defined by a polynomial equation (ref. 14). The airfoils examined in this study had variations in maximum thickness from $0.02c$ to $0.08c$, a maximum-thickness position from $0.2c$ to $0.6c$, and leading-edge radii from 0 to $0.012c$. Perturbations in typical wing geometries were obtained by varying all airfoil parameters both independently and in combinations. Airfoil thickness, maximum-thickness position, and leading-edge radii parametrics were studied in addition to spanwise variations of all the parameters. The airfoil thickness-to-chord ratio was increased in the spanwise direction to create a wing of nearly constant thickness and thus increased the forward-projected area of the wing at the leading edge. The sweep of the airfoil crest line was increased to better align it with the conical flow over the wing upper surface. The airfoil bluntness was reduced inboard to reduce the bow shock and was increased spanwise to control the leading-edge expansion characteristics.
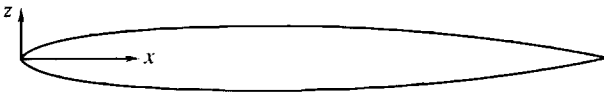
Forward of maximum-thickness location:

$$z = a_0 \sqrt{\frac{x}{c}} + a_1 \frac{x}{c} + a_2 \left(\frac{x}{c}\right)^2 + a_3 \left(\frac{x}{c}\right)^3$$

Aft of maximum-thickness location:

$$z = d_0 + d_1 \left(1 - \frac{x}{c}\right) + d_2 \left(1 - \frac{x}{c}\right)^2 + d_3 \left(1 - \frac{x}{c}\right)^3$$

Leading-edge radius:

$$\frac{r}{c} = \frac{a_0^2}{2} = 1.1019 \left(\frac{t}{c}\right)^2$$

Sketch A

Wing upper and lower surface asymmetry was also investigated as a means to better align the wing streamwise surface slopes with the naturally occurring pressure distribution (fig. 2). Camber and twist were not used to create wing upper to lower surface asymmetry because they would not allow for accurate and independent control of the wing upper and lower surface geometry. The method for wing upper and lower surface asymmetry developed for this study allows for complete control of the wing upper and lower surfaces independent of one another. Wing upper to lower surface asymmetry was created in a two-part process.

Part 1 in the process was directed at increasing the slopes on the upper surface leading edge (forward of the airfoil maximum thickness line). Part 1 was used to modify the cross-sectional surface slopes by redistributing a percentage of the local thickness from the lower surface to the upper surface as defined by a camber function F_c that varies in the streamwise direction (constant at a given cross section). The cross-sectional contour method is depicted in the upper half of figure 2 and shows that the wing leading and trailing edges remain at the same vertical position. However, a result of part 1 is that the magnitudes of all lower surface streamwise slopes are reduced and all upper surface streamwise slopes are increased. Note that this would be less than optimum for the wing upper and lower surfaces in region D as shown in figure 1.

To correct this deficiency, a cross-section shearing method was employed, as part 2, to modify the streamwise surface slopes on the wing in regions that are dominated by streamwise flow. (See the lower half of fig. 2.) The cross-section shearing method was defined such that the cross-sectional thickness at the wing root was centered about the y-axis. The value of the vertical displacement required to center the root thickness of the cross section about the axis is then applied to each point in the cross section. The result of this two-part process for wing surface asymmetry is as follows: symmetric airfoil at the wing root, increased slopes on the wing upper surface leading edge, increased forward-projected area on the wing upper surface, reduced slopes on the wing upper surface aft of the airfoil crest line, and a larger region with aft-facing slopes on the wing lower surface.

Step 1: Preliminary Design Study

The preliminary wing design effort was focused at developing an understanding of the basic aerodynamic characteristics of wings at supersonic speeds. Of particular interest was the influence of wing leading-edge sweep angle and wing airfoil profile.

Based upon the predicted drag results presented in reference 7 and the wing-design space-concept results of reference 8, a baseline standard delta wing (no twist and camber) was established that consisted of a 65° swept leading edge with a 4-percent-thick blunt, modified NACA four-digit airfoil with a maximum thickness located at 20 percent chord.

In addition, if the high-lift, low-lift, and zero-lift drag data of references 7 and 8 are reviewed, a value of $\beta \cot \Lambda$ of 0.6 (composed of a wing leading-edge sweep of 65° and a Mach number of 1.62) would provide an excellent opportunity for high levels of aerodynamic performance. This selection is based upon the rationale that a 65° swept delta wing with an aspect ratio of 1.86 provides a design that balances zero-lift drag and drag due to lift compared with a more slender geometry. (See ref. 8.) At a Mach number of 1.62, the effect of vacuum pressure limit will be minimal, thus providing a 70-percent increase in upper surface lifting potential compared with a 75° swept wing and an 8-percent decrease compared with a 55° swept wing.

The baseline near-conical wing was selected based upon the analysis presented in reference 9. The baseline near-conical geometry (neither twist nor camber) consisted of a 65° swept leading edge with a 4-percent-thick, modified NACA four-digit airfoil with a maximum-thickness position varying linearly in the spanwise direction from $0.2c$ at the wing root to $0.6c$ at 66-percent semispan location. The near-conical wing concept is derived from considerations of matching the wing upper surface geometry to the naturally occurring flow characteristics. A schematic of the near-conical geometry method, which is presented as sketch B, depicts a 65° swept delta wing with a standard airfoil distribution and the near-conical concept of redistributing the airfoils in the spanwise direction to create a near-conical geometry. As shown in sketch B, the resulting wing geometry has two base areas located at the wingtips. These base areas result from truncating the airfoils (which wrap around the airfoil maximum-thickness line) at the wing trailing edge.

Step 2: Initial Design Study

The initial design phase of the study was undertaken using a full-potential code (ref. 12) for the analysis tool. Perturbations in the baseline near-conical wing geometry were made holding the volume to a nearly constant value. The modifications made to the baseline near-conical wings were variations in airfoil thicknesses from $0.02c$ to $0.08c$, maximum-thickness locations from $0.2c$ to $0.6c$, leading-edge

Sketch B
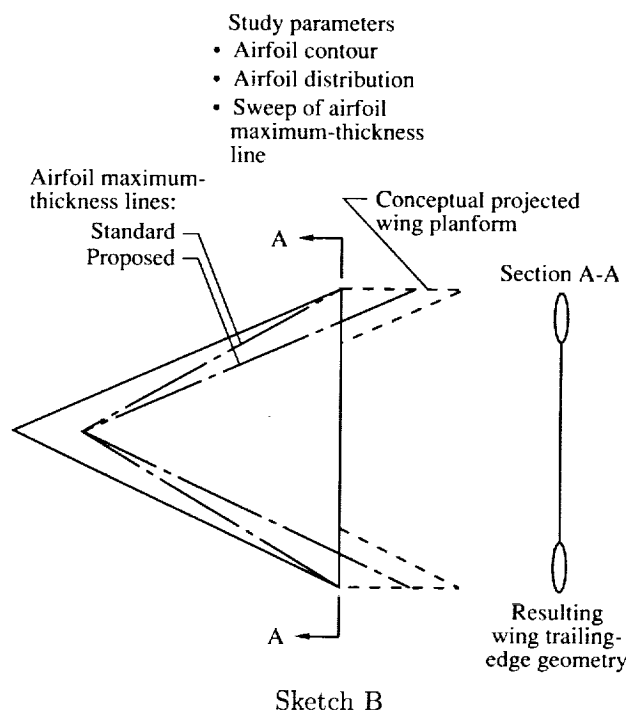
radii from 0 to $0.012c$, and airfoil asymmetry from 0 to 90 percent.

In order to point out the benefits due to this unique wing-design philosophy throughout a large lift range, lift coefficient values of 0.1 and 0.3 were chosen for design points. Presented in figure 3 are predicted aerodynamic characteristics of the baseline standard and the baseline near-conical geometries. The figure shows that the lift characteristics are the same for the near-conical and standard wings; however, the drag was reduced considerably, thereby increasing the L/D of the near-conical wing for both cruise and maneuver lifting conditions ($C_L = 0.1$ and 0.3, respectively). Note that the drag characteristics of the near-conical wing do not include a base drag increment associated with the wingtip base area. A conservative estimate of 0.002 for this coefficient is derived by assuming a base pressure coefficient of -0.2.

The cross-sectional area distributions and the drag buildup for $C_L = 0.1$ for the baseline standard and baseline near-conical configurations are shown in figure 4. The plot of cross-sectional area distribution shows that the near-conical geometry has less volume in the front half of the wing and greater volume in the rear half of the wing compared with the standard wing. As a result, the total volume of the near-conical wing is slightly increased over that of the standard wing. However, the plot of sectional drag shows that the improvements due to the

near-conical geometry compared with the baseline wing are evident over the full length of the wing.

The surface pressure distributions at $x/l = 0.4$ and 1.0 for $C_L = 0.1$ are shown in figure 5. These data illustrate how the spanwise pressure distributions are altered slightly because of geometry modifications, with the primary difference being an increased leading-edge expansion. This increased leading-edge-expansion pressure acting on the modified surface contour for the near-conical geometry results in reduced drag.

The rest of this section of the paper will present the predicted effect of symmetric and asymmetric wing surface contouring between the upper and lower wing surfaces. All modifications have been performed on the near-conical wing, and comparisons between the near-conical wing and the modified near-conical wings will be made.

Wing thickness variation. The natural flow wing-design philosophy suggests that improved aerodynamic performance would result from an increase in airfoil thickness in the spanwise direction by allowing for an increased forward-facing area to be located on the wing upper surface for the low pressures to act upon. To study this effect, a wide range of thickness modifications were computationally evaluated, and selected results from these analyses are presented in figures 6 and 7.

The cross-sectional area distributions and drag distributions in the streamwise direction are presented in figure 6 for the baseline near-conical wing and two modified-thickness near-conical wings having a thickness that varied from the root to the tip of $0.02c$ to $0.08c$ and $0.03c$ to $0.06c$, respectively. In the present study for slender swept wings, the general characteristics of the wing upper surface pressure at all streamwise stations (i.e., the expansion region near the leading edge) are assumed to be nearly independent of the airfoil geometry; therefore, an increase in thickness in the spanwise direction would create an improved surface for the wing upper surface flow to act upon compared with a traditional design. An additional constraint of the thickness study was to maintain a constant wing volume; thus an increase in thickness outboard must be accompanied by a corresponding reduction in the inboard thickness.

The 2- to 8-percent-thick configuration was found to have a reduction in volume of 19.3 percent and at $C_L = 0.1$ a reduction in C_D of 17 counts, and the 3- to 6-percent-thick configuration had a reduction in volume of 4.8 percent with a reduction in C_D of 4.1 counts. Figure 6 illustrates these results; however, the 2- to 8-percent-thick configuration was

rejected because of its large reduction in volume compared with the baseline geometry. A comparison of the drag data of figure 6 shows that the drag reduction resulting from the modified thickness (T(3)) is primarily due to reduced drag at the wing apex $(0 \leq x/l \leq 0.2)$.

Spanwise surface pressure distributions at $x/l = 0.4$ and 1.0 are shown in figure 7 for the baseline near-conical configurations and the modified-thickness near-conical wing with the 3- to 6-percent-thick airfoil distribution. The predicted pressure distributions for the two wings are very similar.

Leading-edge bluntness variation. Changes in leading-edge radius (bluntness) were examined on the baseline near-conical wing. Figure 8 presents the effect on drag due to changes in the leading-edge bluntness at lift coefficients of 0.1 and 0.3. In addition to the leading-edge bluntness variations shown in figure 8, several methods were investigated that reduced the bluntness in the spanwise direction. These tapered bluntness methods had an increase in drag and thus were not considered for further analysis. The data of figure 8 show that increasing bluntness in the spanwise direction reduces the drag for low-lift conditions but has little or no effect at high-lift conditions. At low-lift conditions, the leading-edge expansion is concentrated at the leading edge and combines with the various leading-edge shapes to provide the different drag characteristics. However, at high-lift conditions, the leading-edge expansion extends farther inboard. As a result, the percentage of the leading-edge expansion that acts on the leading edge is significantly reduced, and thus the influence of leading-edge geometry on drag is reduced. The drag data for all modifications show results similar to those observed for the thickness modifications in that the total drag reduction is due primarily to lower drag over the forward portion of the wing. The leading-edge radius modification that has the lowest drag was found to be a variation from 0 at the root to a maximum value of $0.012c$ at the tip.

The surface pressure coefficients are shown in figure 9 for the baseline near-conical wing and the near-conical wing with the leading-edge radius distribution varying from 0 to $0.012c$. A review of the pressure data for these two geometries shows similar trends and levels and supports the observation that the reduced drag for the modified-bluntness wing is primarily due to the reduced apex drag. At $x/l = 0.4$, the full-potential code predicts an expansion followed by an abrupt recompression on the upper surface and an expansion spike on the lower

surface at the leading edge of the modified leading-edge wing (N-C B(1)). This erratic pressure distribution is most likely caused by the inability of the full-potential code to accurately resolve the expanding flow over a wing with a sharp leading edge. The spanwise pressure distribution for the baseline near-conical wing at $x/l = 0.4$ is well-behaved and shows a very gradual expansion at the leading edge on both the lower and upper wing surfaces. At the aft streamwise location ($x/l = 1.0$), where both wings have blunt leading edges, nearly identical pressure loadings are predicted.

As mentioned previously, the method for asymmetric wing surface contour and shearing was developed to allow for detailed control of the wing upper and lower surface geometries during the design process. This is in contrast to typical design methods that warp the wing through twist and camber applied to the mean chord plane. The thickness distribution is then wrapped about the mean chord plane.

Asymmetric wing contouring and shearing. Two approaches were assessed in the application of the asymmetric wing surface contour method to the natural flow wing-design concept. The first approach was to increase the amount of asymmetry in the streamwise direction, referenced to the wing apex, in order to increase the wing leading-edge surface slopes on the outboard portion of the wing to match the increased upwash angle and resultant expansion pressures. The second approach was to impose a constant asymmetry over the complete wing in an effort to control the magnitude of the upwash as it increases in the spanwise direction and, thus, control the flow expansion about the wing leading edge.

The baseline near-conical wing was used as the basis for this initial asymmetric wing contour study. An extensive number of asymmetric wing contours were evaluated in the initial design phase. These analyses identified the constant asymmetric wing contour method as providing improved performance compared with the streamwise variation methods.

Presented in figures 10 and 11 are the predicted lift and drag characteristics for several constant asymmetric wing contour surfaces at lift coefficients of 0.1 and 0.3, respectively. Figure 10 illustrates how changes in wing asymmetry affect the total lift and drag buildup of the near-conical wings. Wing asymmetry is seen to reduce the lift contribution on the forward region of the wing and results in most of the lift coming from the aft region of the wing for low-lift conditions ($C_L = 0.1$).

Although pitching moment is not directly addressed in this study, the aft movement of the lift vec-

tor with wing asymmetry would give a more negative zero-lift pitching moment for all wings and possibly result in an increase in trim drag. The corresponding drag is seen to decrease slightly for the 20-percent asymmetric configuration and increase for configurations with greater asymmetry compared with the baseline near-conical wing.

At the high-lift condition ($C_L = 0.3$ in fig. 11), the 90-percent asymmetric configuration was found to obtain significantly greater lift and drag in the forward region of the wing than the other three configurations. The drag buildup data of figure 11 show that the 20-percent asymmetric wing has lower drag compared with the other wings. The large increase in drag with large amounts of asymmetry predicted by the full-potential method is a result of the inability of the codes to resolve the flow about a sharp leading edge. The increase in drag with increasing wing asymmetry and the increased lift loading on the forward portion of the 90-percent asymmetric wing at the high-lift condition compared with the near-conical baseline wing raises doubts about the ability of the full-potential method to accurately resolve the flow field about these sharp leading-edge wings. (See sketch C.) Note that as wing asymmetry is increased, the wing leading edge begins to develop a reduced leading-edge radius on the lower half of the leading edge and an increased leading-edge radius on the upper half of the leading edge. (See sketch C.)

The surface pressure coefficient (C_p) distributions are shown in figure 12 for the $C_L = 0.1$ condition at $x/l = 0.4$ and 1.0 for the near-conical and the 90-percent asymmetric near-conical configurations. Results from the full-potential solver show that at $x/l = 0.4$, the configuration has more negative C_p values on the lower surface at the leading edge than on the upper surface. The large spikes in the C_p data at the leading edge of the wing are often seen in the data from this code because of difficulties in solving the full-potential equations near regions where the geometry changes rapidly, i.e., sharp leading edges. In order to resolve these discrepancies, additional analysis of the asymmetric wings will be performed with the Euler solver in the final phase of the study in order to minimize errors obtained at the leading edge of the wing. (See the appendix.)

Step 3: Final Design Study

The wing geometry variables in the final design study were selected based upon the full-potential results obtained in the initial design phase of the study. A constant wing thickness of 4 percent and a wing thickness that varied linearly from 3 percent at the
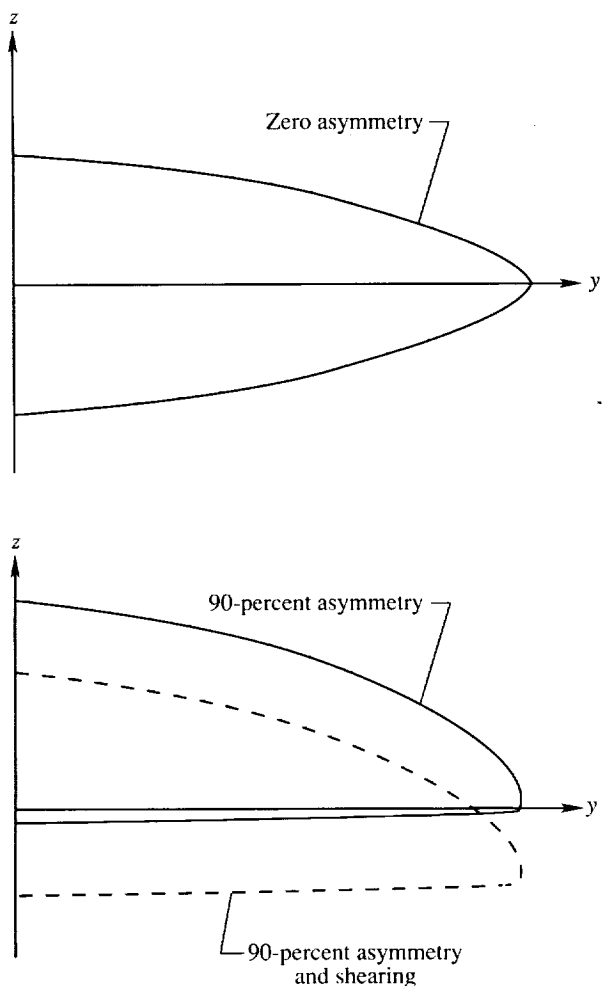
Sketch C

root to 6 percent at the tip were selected for further evaluation. The near-conical method initially employed was maintained, and two leading-edge bluntness distributions were selected. The first bluntness was a constant $0.009c$ and the second varied between 0 and $0.012c$ along the span. Wing asymmetry and shearing was the only geometry variable that was extensively studied in the final design phase.

The full-potential results obtained in the initial design phase failed to provide a clear understanding of the influences of wing asymmetry on the aerodynamic performance of the wings. As a result, an in-depth evaluation was performed with the Euler method in which both constant and varying asymmetric contouring and shearing methods were evaluated. The Euler analysis presented in figures 13–23 confirmed the full-potential results which concluded that only the constant asymmetry methods provide improved aerodynamic performance at both the low-lift and high-lift conditions.

Presented in figures 13 and 14 are Euler-predicted lift and drag buildup plots for wings with 20-, 50-, and 90-percent asymmetry at lift coefficients of 0.1 and 0.3, respectively. A comparison of the Euler-predicted pressure distributions and flow field characteristics with the full-potential results shows that the Euler results are smooth and continuous about the leading-edge region whereas the full-potential results are erratic. (See figs. 12 and 22.) As a result of this analysis it was concluded that the Euler method provides an improved model of the flow about the wing. At low lift, the 50- and 90-percent asymmetric wings showed large reductions in drag. At high lift, the 20- and 50-percent asymmetric wings showed small reductions in drag, and the 90-percent asymmetric wing again showed large reductions in drag. The drag reduction at the high-lift condition was expected; however, the increased drag reduction with increased wing asymmetry at low lift was not expected. Based upon the Euler analysis results presented in figures 13 and 14, the 90-percent constant asymmetry was selected for further analysis.

Thickness and leading-edge bluntness modifications were also studied in this phase of the design and resulted in the selection of a leading-edge bluntness variation from 0 to $0.012c$ (B(1)) and a thickness variation of 3 to 6 percent (T(3)). Shown in figure 15 are cross-section cuts and streamwise cuts through the baseline standard wing, baseline near-conical wing, and the baseline near-conical wing with bluntness, thickness, and asymmetry modifications. Cross-section cuts are presented for $x/l = 0.25, 0.50, 0.75$, and 1.00, and streamwise cuts are presented for $2y/b = 0, 0.2, 0.4, 0.6$, and 0.8. The sketches in figure 15 show that the near-conical wing has an increased thickness in the spanwise direction, compared with the standard wing, that creates an increase in leading-edge bluntness on the outboard portion of the wing and thus an improved surface for the flow to expand about.

The selected leading-edge bluntness modification (B(1)) has a reduced bluntness at the wing apex and an increased bluntness on the outboard portion of the wing. This modification results in reduced drag because of a combination of lower pressures at the apex and reduced forward-facing slopes on the leading-edge lower surface which the positive pressures act on.

The selected wing thickness modification (T(3)) has reduced thickness inboard and increased thickness-to-chord ratio outboard compared with the baseline near-conical wing. This results in a geometry that has increasing leading-edge bluntness in the spanwise direction. The modified-thickness wing

has a nearly constant dimensional thickness and an increased bluntness in the spanwise direction; thus it is well-tailored to the naturally occurring near-conical upper surface flow.

The near-conical method and the selected bluntness and thickness modifications were directed at contouring the wing leading edge and upper surface geometry, and this resulted in symmetric wings. In an effort to modify the wing lower surface geometry while maintaining the preferred upper surface characteristics, the wing asymmetric contouring and shearing method was used. The mathematical modeling method selected for the study did not allow for an independent design of the wing upper and lower surfaces; however, the method did allow the desired character for each surface to be developed in the design process. The selected asymmetric wing geometry has 90-percent volumetric asymmetry at each cross section. The asymmetric wing has a large region of aft-facing slopes on the lower surface, reduced aft-facing slopes on the upper surface rearward of the airfoil crest line, and increased forward-facing slopes on the upper surface in front of the airfoil crest line.

The predicted aerodynamic characteristics of the selected thickness and bluntness modifications along with those for 90-percent asymmetry are shown in figures 16-18. At low-lift conditions (fig. 16), it was found that modifying the thickness resulted in the largest reduction in drag; whereas wing asymmetry and modifying the leading-edge bluntness provided only small reductions compared with the baseline near-conical wing. At high lift (fig. 17), asymmetry provides the largest reduction in drag compared with the baseline near-conical wing. The data in figure 18 show that the thickness modification yields the highest $(L/D)_{max}$, which occurs near $C_L = 0.15$. At higher values of C_L, the asymmetric wing has the best performance.

All analysis results presented previously were for single geometry modifications to the baseline near-conical wing. The final step in the design process was to combine the various geometry modifications to further refine the wing. A comparison between the baseline wing, the baseline near-conical wing, and the final design natural flow wing is presented in figures 19-23. The final design natural flow wing is defined by a near-conical airfoil distribution that varies from a maximum thickness position of $0.2c$ at the root to $0.6c$ at 0.66 semispan positions. The thickness distribution varies from $0.03c$ at the root to $0.06c$ at the tip, and the leading-edge radius varies from 0 at the root to $0.012c$ at the tip. The selected wing asymmetry is a constant 90 percent and sheared.

Cross-section spanwise cuts and streamwise cuts through the baseline standard, baseline near-conical, and natural flow wings are shown in figure 19(a). The sketches show that the combination of a near-conical airfoil distribution with the selected bluntness, thickness, and asymmetry modifications creates a three-dimensional wing geometry that is well-tailored to match the naturally occurring flow field, as discussed previously. To provide additional insight into the three-dimensionality of the geometry, elevation cuts through the three wings are presented in figure 19(b). Note that both the baseline standard and baseline near-conical wings are symmetric about the horizontal plane. The elevation cuts show that the near conical wing has a significantly improved upper surface geometry compared with the standard wing; however, the lower surface of the near-conical wing is not properly contoured to match the expected constant pressures.

As discussed previously, the lower surface of the wing should have aft-facing slopes to take advantage of the positive pressures in reducing the drag and creating lift. A review of the natural flow wing geometry shows an upper surface that has a nearly constant leading-edge shape along the entire span. Figure 19(b) shows that the upper surface forward-sloping area is increased and the upper surface rearward-sloping area is decreased compared with the near-conical wing. The elevation cuts for the natural-flow wing also show that the lower surface geometry is dominated by a large region with a rearward slope, thus providing a much improved surface compared with the standard and near-conical wings.

Figures 20 and 21 illustrate the lift and drag buildup for the baseline standard, baseline near-conical, and natural flow wings at lift coefficients of 0.1 and 0.3, respectively. The results presented in figures 20 and 21 show that the natural flow wing when compared with the baseline near-conical wing has significantly lower lift over most of the wing, but there is a significant increase in the sectional lift (as indicated by the increased slope in the plot of C_L against x/l) over the final 10 to 15 percent of the wing. This increase in the sectional lift results in a similar increase in the sectional drag at the trailing edge of the natural flow wing. A review of the lift and drag buildup results for the isolated geometry modifications (see figs. 16 and 17) shows that the increases in drag and lift at the trailing edge are due primarily to asymmetry. A review of the wing geometry (figs. 15 and 19) shows that the combination of asymmetry with the near-conical method not only produces the desired large forward-facing streamwise

slopes on the upper surface but also creates a region of aft-facing area near the trailing edge on the upper surface located inboard of $y/(b/2) = 0.78$. The predicted surface pressure data of figure 22 show that this aft-facing region produces an additional expansion over the upper surface inboard region of the wing at the trailing edge which combines with the aft-facing upper surface to create a drag increase. This increase in drag is shown in figure 20 by the abrupt increase in slope in the plot of $C_{D,I}$ against x/l for the natural flow wing.

The Euler-predicted longitudinal aerodynamic characteristics of the baseline, near-conical, and final design natural flow wings are presented in figure 23. The plot of lift against angle of attack shows that all three wings vary linearly for lift coefficients up to 0.3 and have nearly equivalent lift-curve slopes. The data in figure 23 show that the final design natural flow wing has higher L/D values and lower drag compared with the baseline near-conical wing for lift coefficients greater than 0.05. Compared with the standard wing, the natural flow wing produced a drag reduction of 0.0012 at the low-lift condition and of 0.0060 at the high-lift condition. Note that the base drag increment mentioned earlier would tend to reduce the magnitude of these benefits. Compared with the baseline near-conical wing, the natural flow wing provides a drag reduction of 0.009 at a lift coefficient of 0.1 and of 0.0050 at a lift coefficient of 0.3.

The large drag reductions achieved at lifting conditions are a result of improvements in the drag-due-to-lift characteristics as well as a reduction in zero-lift drag for the natural flow wing design compared with the baseline near-conical and standard wings. The predicted L/D characteristics show that the natural flow design provides a 15-percent improvement in maximum L/D compared with the baseline standard design and a 10-percent improvement compared with the baseline near-conical design. The natural flow wing was found to reduce the drag coefficient from the baseline and near-conical wings by 13 percent and 10 percent, respectively, at a lift coefficient of 0.1 and by 14 percent and 12 percent, respectively, at a lift coefficient of 0.3.

Comparison of Natural Flow Design With Linear-Theory Cambered Design

To further evaluate the relative merits of the natural flow design, a cambered wing derived by linear theory has been developed and analyzed with the Euler method of reference 13. In order to fully assess the merits of linear-theory design methods, a state-of-the-art, linear-theory wing-design method that accounts for nonlinear flow effects, leading-edge thrust, and vortex flow was selected for the design. (See ref. 15.) The linear-theory cambered-design process was conducted on a baseline standard wing at a series of lift coefficients between 0 and 0.3. Neither pitching moment nor geometry constraints were imposed in the design process so as not to restrict the drag reduction potential of the design. The linear-theory-predicted performance of all designs was then compared and evaluated over the lift coefficient range from 0 to 0.3. Based upon this analysis, the camber surface at $C_L = 0.16$ was selected as best and would be evaluated with the Euler method of reference 15.

Sketches of the geometries of the natural flow wing and linear-theory cambered wing are presented in figure 24. A review of the cross-section cuts for the two wings shows that the linear-theory wing is severely warped compared with the natural flow wing. This large amount of wing warp is typical of linear-theory designs and results from the tendency of these methods both to distribute the predicted loading equally between the wing upper and lower surface and to align the wing leading edge into the upwash field. Despite the extreme warpage of the linear-theory design, a close examination of the geometry of the two wings shows that the natural flow wing has an increased upper surface forward-facing area for values of x/l between 0 and 0.5 and a reduced upper surface forward-facing area for values of x/l greater than 0.6. The combination of the larger upper surface forward-facing area (increased leading-edge thrust) and the flat lower surface geometry for the natural flow wing compared with the linear-theory wing should provide improved performance at all lift conditions.

The Euler-predicted cross-sectional lift and drag coefficient distributions for the natural flow and linear-theory cambered wings are shown in figures 25 and 26 for lift coefficients of 0.1 and 0.3, respectively. A comparison of the lift distributions of 0.1 and 0.3 for each wing shows that they follow the same trends. The lift data show that the natural flow wing is more aft-loaded than the linear-theory design which has a near-linear distribution. A further review of the wing geometry sketches of figure 24 shows that the reduced loading at the wing apex ($x/l = 0.1$) of the natural flow wing is due to the increased wing leading-edge upper surface slopes compared with the linear-theory wing. The increased slopes would reduce the leading-edge expansion and resultant upper surface loading at this x/l location. Additionally, the upwash field would be significantly reduced. A further review of the geometry presented in figure 24 shows that the leading-edge droop of the linear-theory wing

increases along the span (increasing x/l) from 0 to a very large negative angle. The result of this geometry is that at low-lift conditions, the linear-theory wing would be more highly loaded at the apex than the natural flow wing; and as lift would increase, the streamwise loading on the linear-theory wing would become a nearly constant level similar to that observed for the natural flow wing.

Linear-theory and Euler-predicted drag characteristics for the baseline standard wing, linear-theory cambered wing, and natural flow wing are presented in figure 27. Also shown for comparison are linear-theory predictions for cambered designs with $C_L = 0.1$ and 0.3. Note that the linear-theory results of figure 27 include both leading-edge thrust and vortex flow increments. The results presented in figure 27 show that the natural flow design has lower drag at $C_L = 0.1$ and 0.3 than all other wings shown. Euler-analysis results for the baseline standard wing compare well with the linear-theory results because of the mild surface curvatures. However, the Euler analysis of the linear-theory design clearly shows a significant loss in performance at high-lift conditions from that expected from linear-theory estimates. These analyses show that the performance of the highly warped (twist and camber) wings produced by linear-theory design methods is severely degraded as the wing pressure loading is increased and begins to violate the linear-theory assumptions. The natural flow wing was found to reduce the drag coefficient from the linear-theory wing by 2 percent at a lift coefficient of 0.1 and by 10 percent at a lift coefficient of 0.3. Again, it should be noted that no base drag penalty for the natural flow wing has been included in the comparisons.

Concluding Remarks

A novel wing-design concept is presented in which a natural flow wing-design approach is employed that uses a near-conical thickness distribution to match the wing upper surface contour to the conical nature of the flow at supersonic speeds. In previous studies conducted by the authors, the description of the delta-wing planform selection criteria, the design Mach number selection criteria, and the near-conical

wing-design philosophy were presented and applied to flat wings. The present study is an extension of the previous effort to include variations in maximum-thickness location, thickness, leading-edge bluntness, and wing asymmetry.

An initial design phase employed a nonlinear full-potential analysis method to assess the merits of the natural flow design approach as well as the effect of thickness, bluntness, and wing asymmetry modifications. However, if the leading edge does become sharp (as is the case for the highly asymmetric geometries and for low values of leading-edge radius), the full-potential analysis is questionable. Therefore, in order to more accurately predict leading-edge effects, an Euler analysis method was employed; and the resulting benefits due to modifications in geometry were assessed and rated for overall performance.

A "natural flow" wing, which was a combination of the optimum thickness, bluntness, and asymmetry modifications, was analyzed using the Euler method and compared with the baseline standard wing, the baseline near-conical wing, and a wing developed using linear-theory design methods. The natural flow wing was found to reduce the drag coefficient from the baseline, near-conical, and linear-theory-designed wings by 13 percent, 10 percent, and 2 percent, respectively, at a lift coefficient of 0.1 and by 14 percent, 12 percent, and 10 percent, respectively, at a lift coefficient of 0.3. These values do not take into account a base drag penalty that would be present for the near-conical and natural flow wings. An accurate determination of this penalty will require experimental measurements.

Acknowledgment

Appendix
Theoretical Analysis Methods

The initial theoretical analysis was conducted with the full-potential method of reference 12, and the final theoretical analysis used the Euler method of reference 13; both were developed by Rockwell International under a grant with the NASA Langley Research Center. The input geometry and grid generation are common to both codes and allow for a straightforward comparison of the results from the two analysis tools. Skin-friction drag was calculated by using the method described in reference 16 and added to the inviscid drag predictions from the full-potential and Euler routines.

The full-potential code employs the conservative, steady form of the full-potential equations developed to solve predominantly supersonic flow with embedded subsonic regions. The theory of characteristics is used to monitor the type-dependent flow field, and a conservative switching method handles the transition between the supersonic marching algorithm and the subsonic relaxation procedure. The finite-differenced equations are solved by using an implicit approximate factorization method. A finite-volume, multizone implementation of a total variation-diminishing (TVD) formulation (based on Roe's method in ref. 17) is used to solve the Euler equations across the entire Mach number range. An infinitely large time step (causing the transient terms in the discretized equations to vanish) and a space-marching method are used in supersonic regions of the flow; a finite time step and a relaxation method are used in subsonic flow regions.

The wing geometries are defined using a routine written by the authors which takes advantage of the analytic description of the modified NACA four-digit airfoils. The wings can be easily generated with the capability for varying airfoil maximum-thickness location, airfoil thickness, leading-edge bluntness, wing asymmetry, and leading-edge sweep. The wing geometry definition is input to the code as a set of discrete points in a crossplane at various streamwise locations and is identical for both the full-potential and Euler codes. The griding routine inside each code then divides the cross-sectional input points into several patches using a cubic spline routine to define the surface within each patch. The desired grid clustering is then set up on the body surface. An elliptic grid generator is implemented to generate the grid for the flow field calculations between the body surface and an appropriately chosen outer boundary.

The number of patches, points per patch, and points in the normal direction could be varied to cluster the grid in regions where more refinement to the grid was necessary. The full-potential code was executed on the Control Data Corporation VPS-32 computer on a 4-patch grid with 12 points in the first and fourth patches and 20 points in the second and third patches with 22 points in the normal direction and 20 input geometry planes. (See fig. A1(a).) The average execution time was approximately 140 Central Processing Unit (CPU) sec. The full-potential code was also run on a Cray Y-MP computer. Initially, the same gridding method was employed and average CPU times were from 20 to 70 sec. A refined grid with 3 patches (20 points in the first and third patches and 30 points in the second patch) and 100 input geometry planes (fig. A1(b)) varied in CPU time from 200 to 700 sec depending on angle of attack. The significant increase in CPU time was mainly due to increased input/output (I/O) time. The Euler solver, with the three-patch refined grid mentioned previously, had execution times that averaged between 300 and 1300 CPU sec. Euler results were obtained for the linear-theory-designed wing with a four-patch grid. The 4-patch grid had 28 points in the first and fourth patches and 9 points in the second and third patches. The second and third patches were applied locally at the wing leading edge in order to provide a high definition of the thin geometry.

Both codes were modified to print out sectional values of lift, drag, and pitching-moment coefficients as well as the longitudinal summation of these values. This was done so that the effect on the forces due to geometry modification could be better understood. This then allowed the authors to determine which modifications provided the most drag reduction in the wing design. Both codes were modified to output incremental force and moment buildups as well as cross-sectional area, wetted area, and volume.
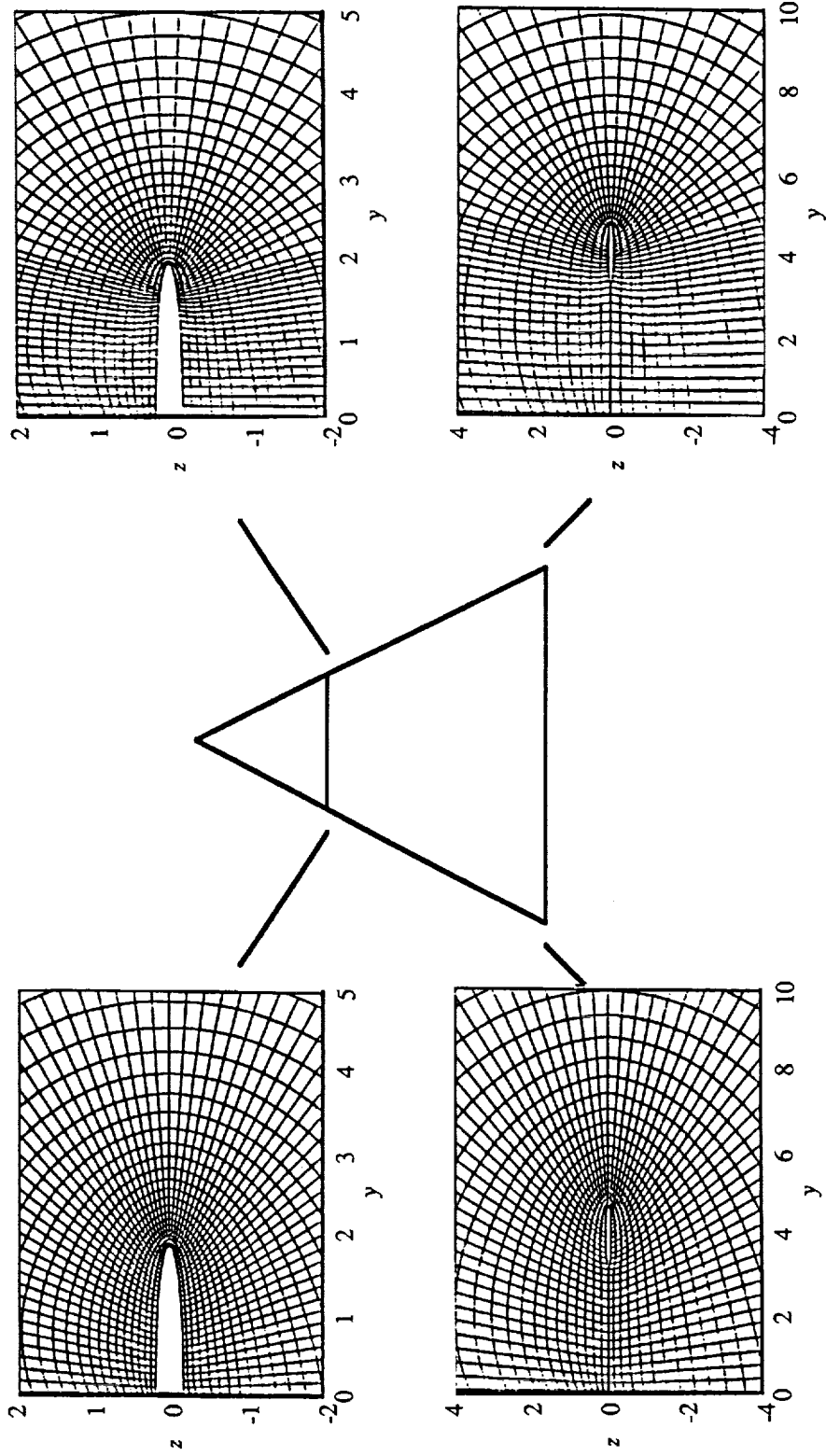
(a) Full-potential code. Grid: $64 \times 22 \times 20$.

(b) Euler code. Grid: $70 \times 22 \times 100$.

Figure A1. Representative grids used in computational study of near-conical wing.

12

References

1. Jameson, Antony: Iterative Solution of Transonic Flows Over Airfoils and Wings, Including Flows at Mach 1. *Commun. Pure & Appl. Math.*, vol. XXVII, no. 3, May 1974, pp. 283–309.

2. Woodward, F. A.: *An Improved Method for the Aerodynamic Analysis of Wing-Body-Tail Configurations in Subsonic and Supersonic Flow.*
   Part I—Theory and Application. NASA CR-2228, Pt. I, 1973.
   Part II—Computer Program Description. NASA CR-2228, Pt. II, 1973.

3. Carlson, Harry W.; and Miller, David S.: *Numerical Method for the Design and Analysis of Wings at Supersonic Speeds.* NASA TN D-7713, 1974.

4. DeCamp, Ronald W.; and Hardy, Richard: Mission Adaptive Wing Advanced Research Concepts. *AIAA Atmospheric Flight Mechanics Conference—A Collection of Technical Papers, Aug. 1984*, pp. 465–470. (Available as AIAA-84-2088.)

5. Covell, Peter F.; Wood, Richard M.; and Miller, David S.: *Investigation of Leading-Edge Flap Performance on Delta and Double-Delta Wings at Supersonic Speeds.* NASA TP-2656, 1987.

6. Mason, W. H.; Siclari, M. J.; Miller, D. S.; and Pittman, J. L.: A Supersonic Manuever Wing Designed for Nonlinear Attached Flow. AIAA-83-0425, Jan. 1983.

7. Wood, Richard M.; and Miller, David S.: Impact of Airfoil Profile on the Supersonic Aerodynamics of Delta Wings. AIAA-85-4073, Oct. 1985.

8. Wood, Richard M.: *Supersonic Aerodynamics of Delta Wings.* NASA TP-2771, 1988.

9. Wood, Richard M.; and Bauer, Steven X. S.: Evaluation of a Three-Dimensional Empirically Derived Wing at Supersonic Speeds. AIAA-88-0481, Jan. 1988.

10. Bauer, Steven X. S.; Wood, Richard M.; and Brown, S. Melissa: A Natural Flow Wing Design Employing 3-D Nonlinear Analysis Applied at Supersonic Speeds. AIAA-89-2167, July/Aug. 1989.

11. Siclari, Michael J.: *The NCOREL Computer Program for 3D Nonlinear Supersonic Potential Flow Computations.* NASA CR-3694, 1983.

12. Shankar, Vijaya; Szema, Kuo-Yen; and Bonner, Ellwood: *Full Potential Methods for Analysis/Design of Complex Aerospace Configurations.* NASA CR-3982, 1986.

13. Szema, Kuo-Yen; Chakravarthy, Sukumar; and Shankar, Vijaya: *Supersonic Flow Computations Over Aerospace Configurations Using an Euler Marching Solver.* NASA CR-4085, 1987.

14. Abbott, Ira H.; and Von Doenhoff, Albert E.: *Theory of Wing Sections.* Dover Publ., Inc., c.1959.

15. Carlson, Harry W.; and Walkley, Kenneth B.: *Numerical Methods and a Computer Program for Subsonic and Supersonic Aerodynamic Design and Analysis of Wings With Attainable Thrust Considerations.* NASA CR-3808. 1984.

16. Sommer, Simon C.; and Short, Barbara J.: *Free-Flight Measurements of Turbulent-Boundary-Layer Skin Friction in the Presence of Severe Aerodynamic Heating at Mach Numbers From 2.8 to 7.0.* NACA TN 3391, 1955.

17. Roe, P. L.: Approximate Riemann Solvers, Parameter Vectors, and Difference Schemes. *J. Comput. Phys.*, vol. 43, no. 2, Oct. 1981, pp. 357–372.

Region	Surface slope	Pressure	Drag
A	Positive	High	High
B	Positive	Low	Low
C	Negative	Low	High
D	Negative	High	Low

Expansion region

Compression region

Airfoil maximum-thickness line

Cross-flow recompression line

Upper surface

Standard wing

Natural flow wing

Lower surface

Standard wing
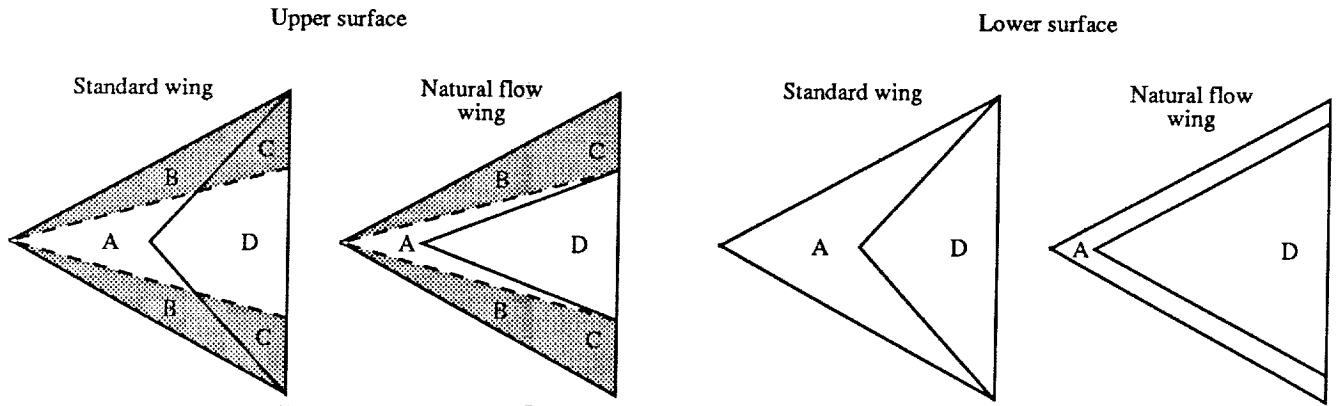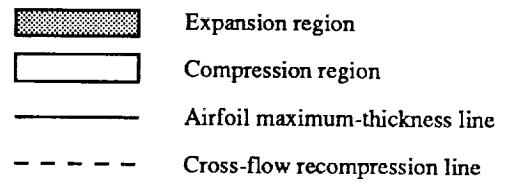
Natural flow wing

Figure 1. Illustration of natural flow wing-design concept.

Spanwise variation

Chordwise variation

x/l

l

No asymmetry

Asymmetry

$$F_c = \left(1 - \frac{x}{l}\right)\left(\frac{\Delta t}{t}\right)_{\text{apex}} + \left(\frac{x}{l}\right)\left(\frac{\Delta t}{t}\right)_{\text{TE}}$$

$$y_{\text{upper}} = t\left(F_c + \tfrac{1}{2}\right)_{\text{upper}}$$

$$y_{\text{lower}} = t\left(F_c + \tfrac{1}{2}\right)_{\text{lower}}$$

Shearing

$$\Delta t_s = t_{\text{C}} F_c$$

$$y = y - \Delta t_s$$
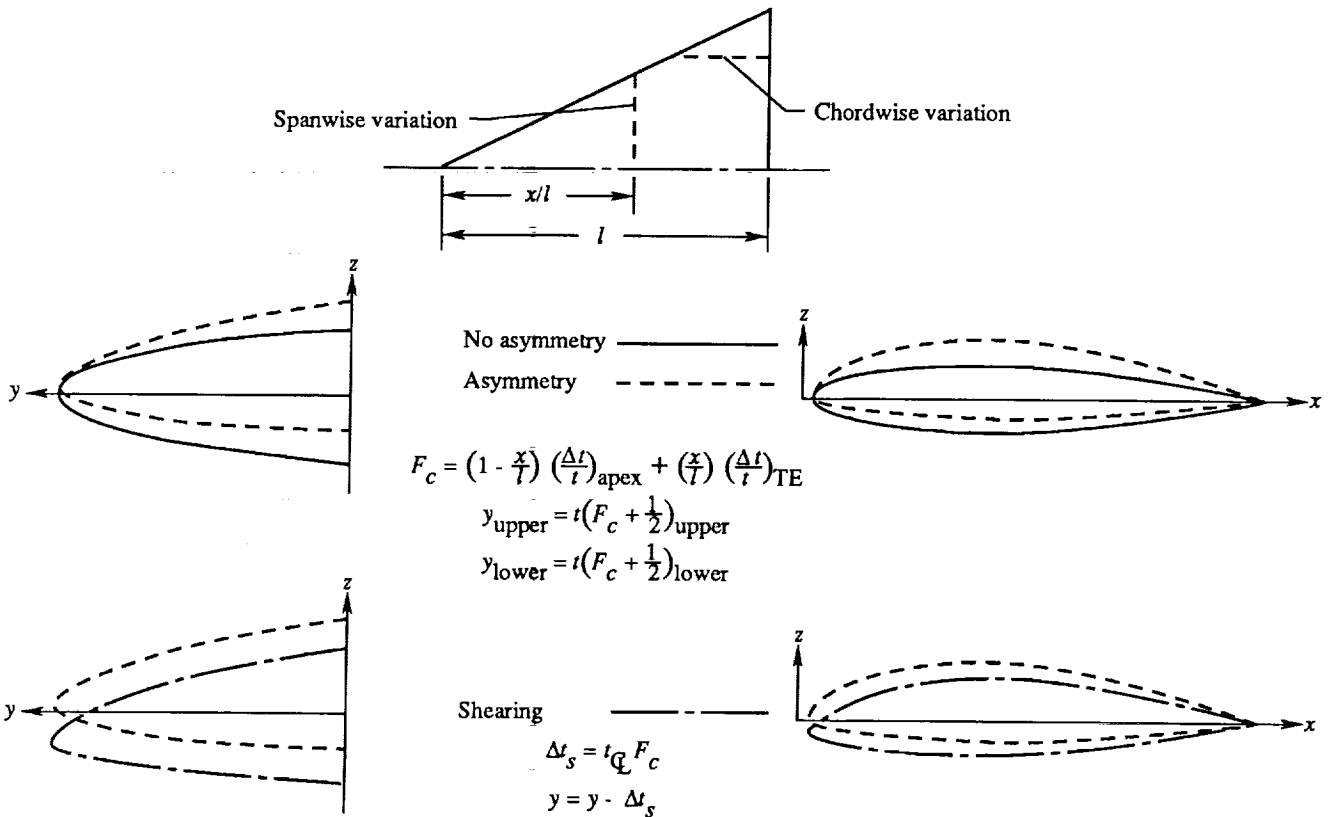
Figure 2. Wing asymmetry and shearing method.
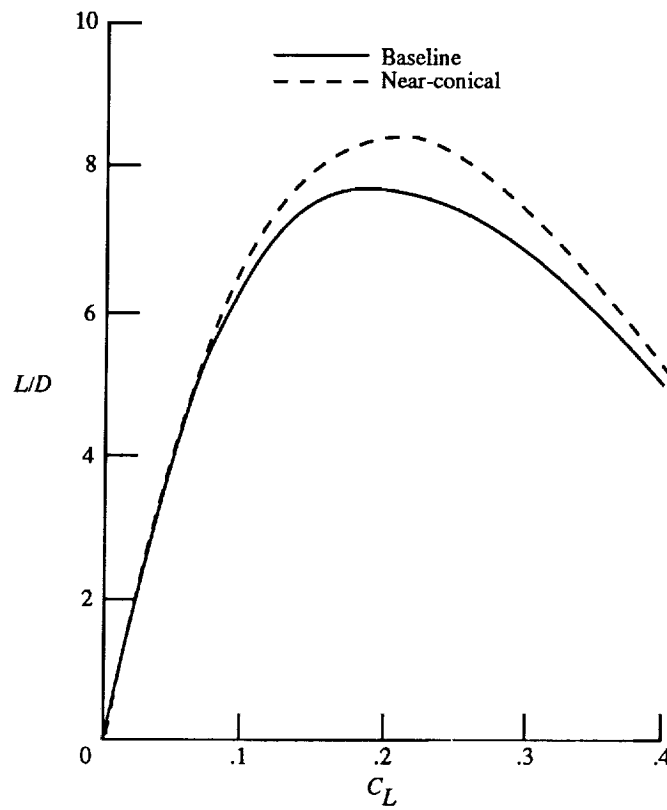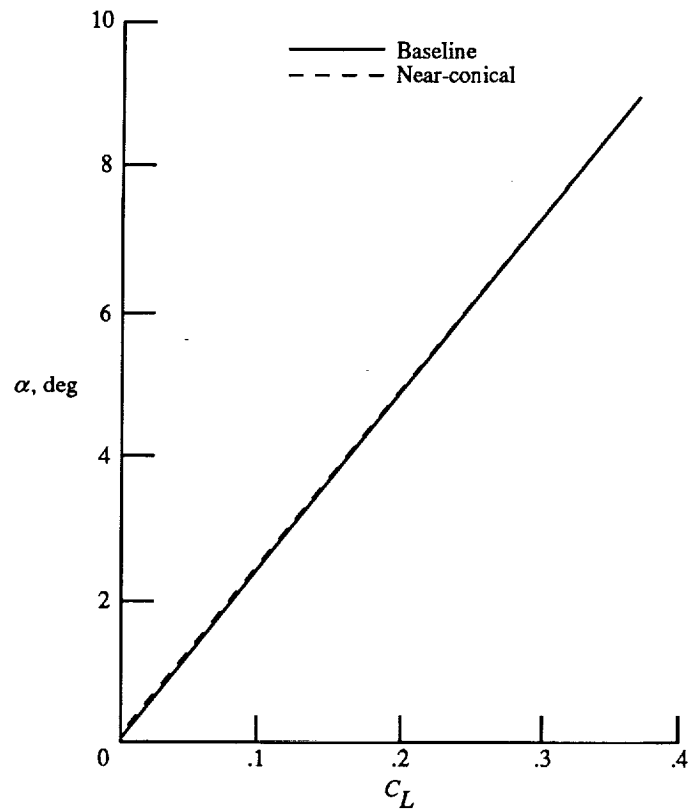
Figure 3. Full-potential predicted aerodynamic characteristics of baseline standard and baseline near-conical wings for $M = 1.62$.
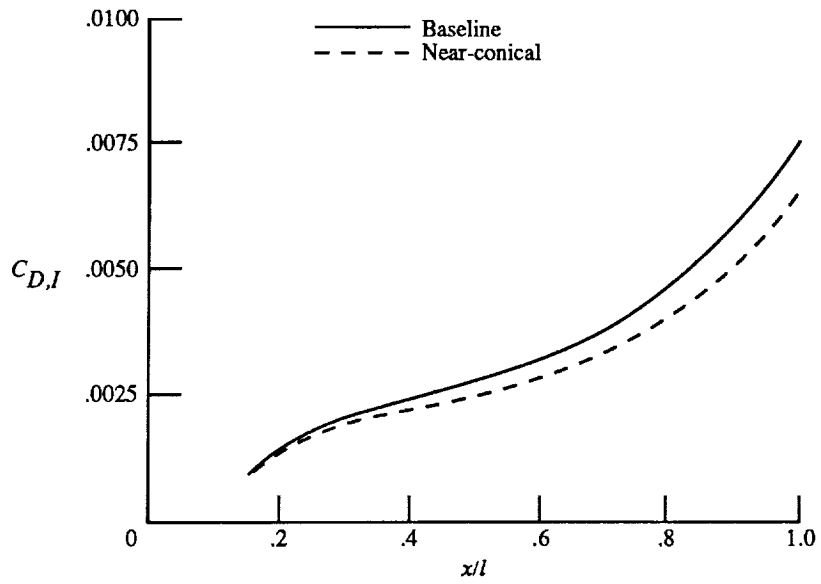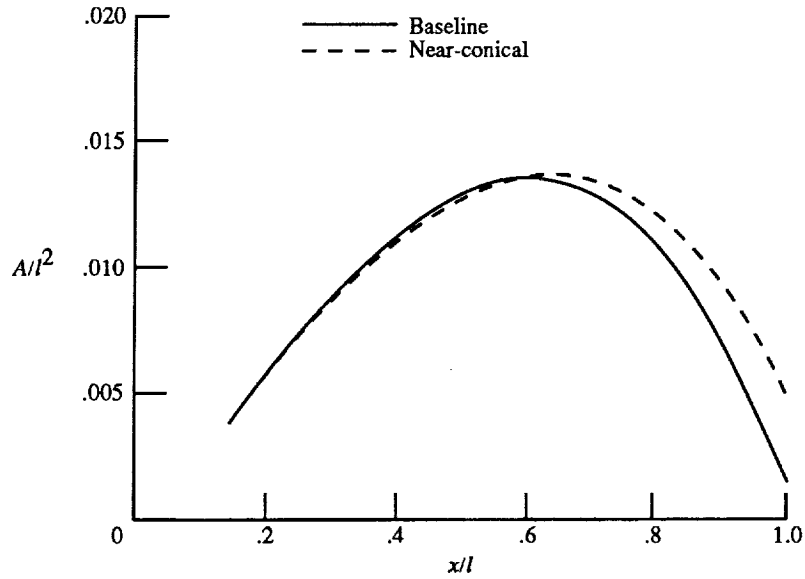
Figure 4. Cross-sectional area and full-potential predicted drag buildup for baseline standard and baseline near-conical wings for $M = 1.62$ and $C_L = 0.1$.
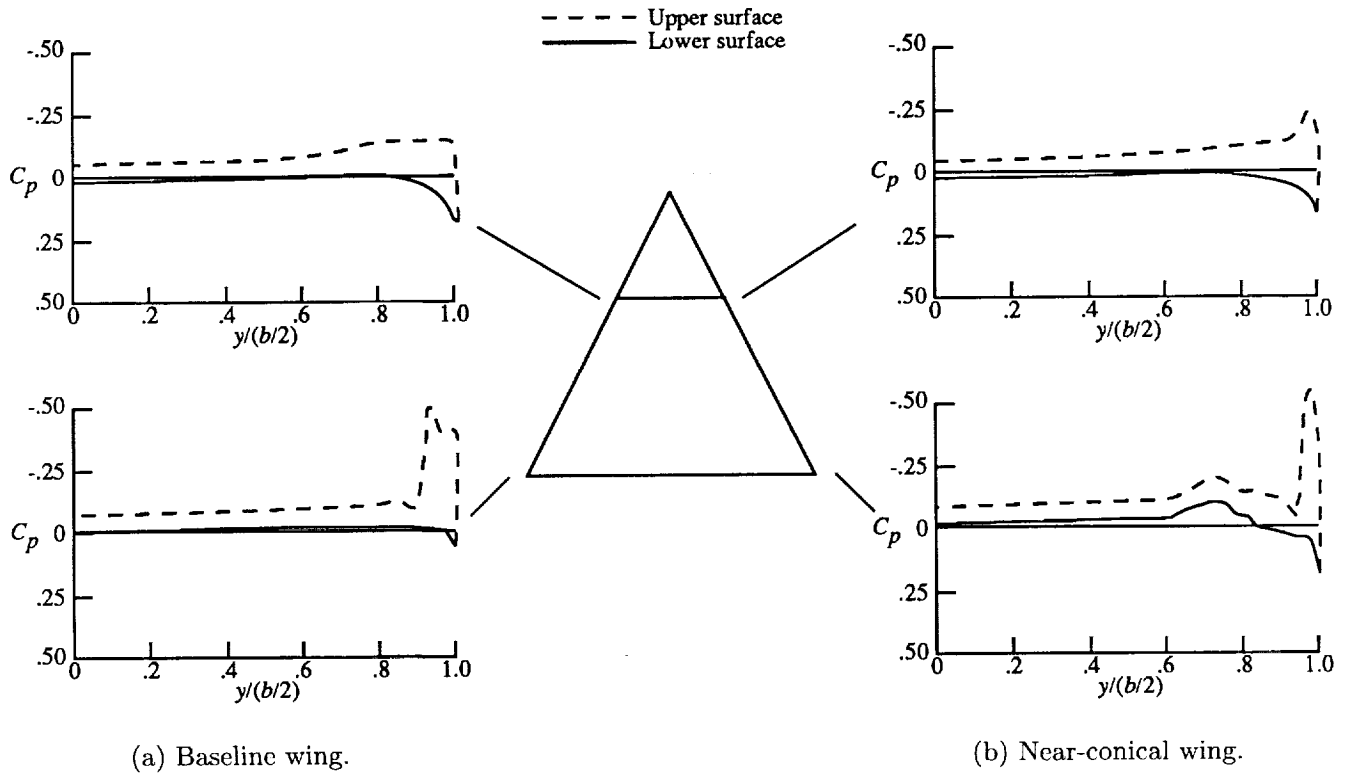
Figure 5. Full-potential predicted surface pressure distributions for baseline standard and baseline near-conical wings at $x/l = 0.4$ and 1.0 for $M = 1.62$ and $C_L = 0.1$.

(a) Baseline wing.
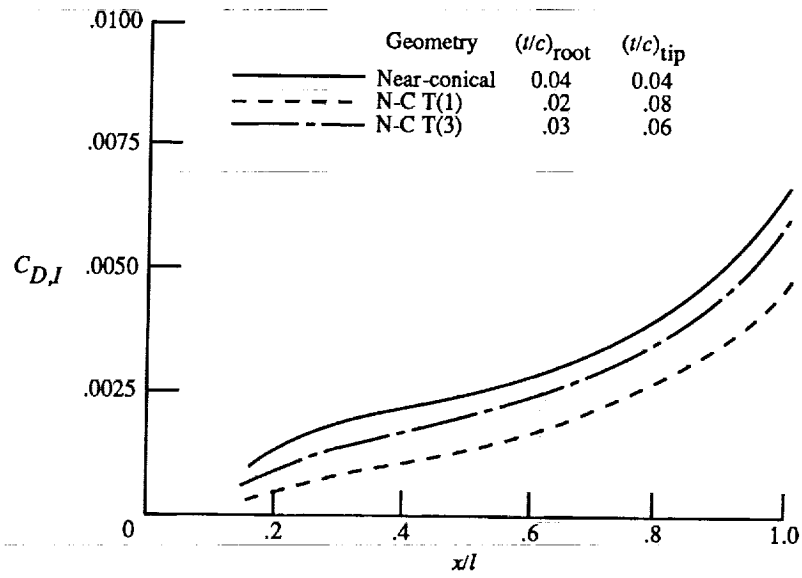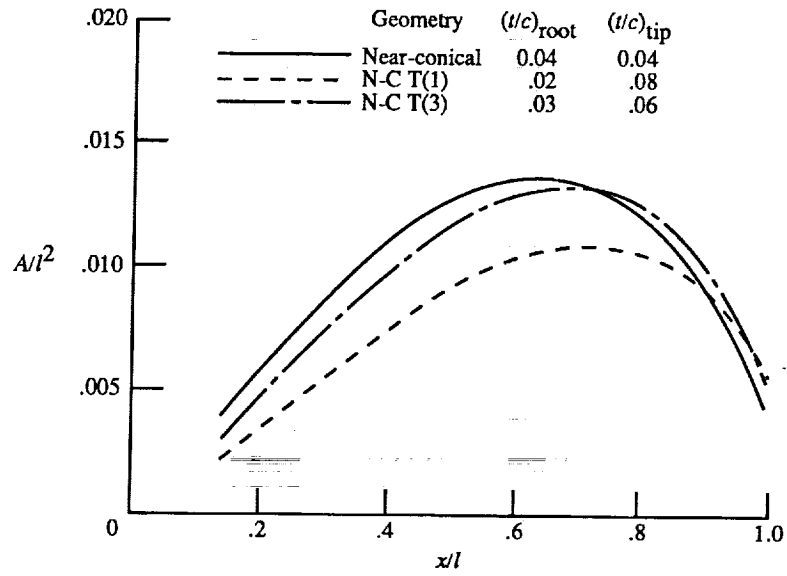
(b) Near-conical wing.

Figure 6. Cross-sectional area and full-potential predicted drag buildup for variations in airfoil thickness for $M = 1.62$ and $C_L = 0.1$.
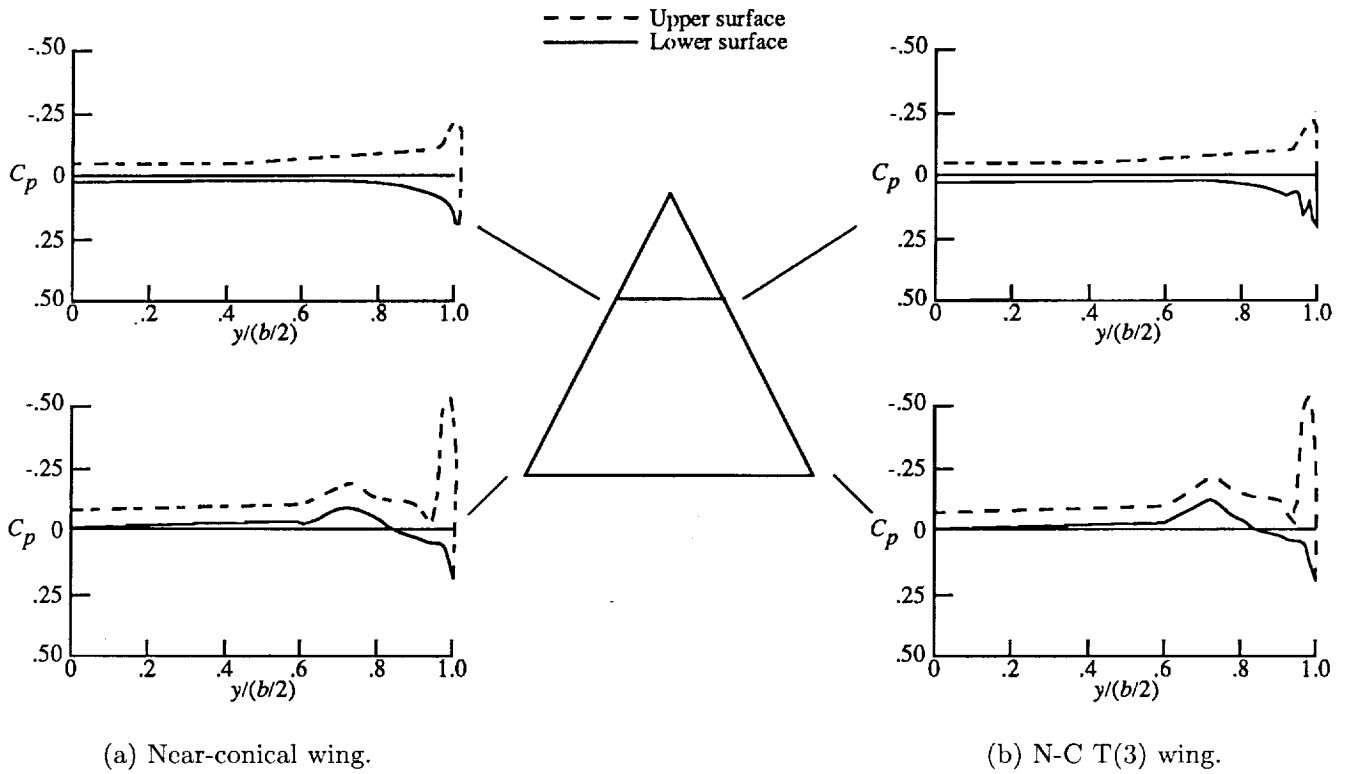
Figure 7. Full-potential predicted surface pressure distributions for near-conical wing and near-conical wing with airfoil thickness variation from 0.03c to 0.06c at $x/l = 0.4$ and 1.0 for $M = 1.62$ and $C_L = 0.1$.
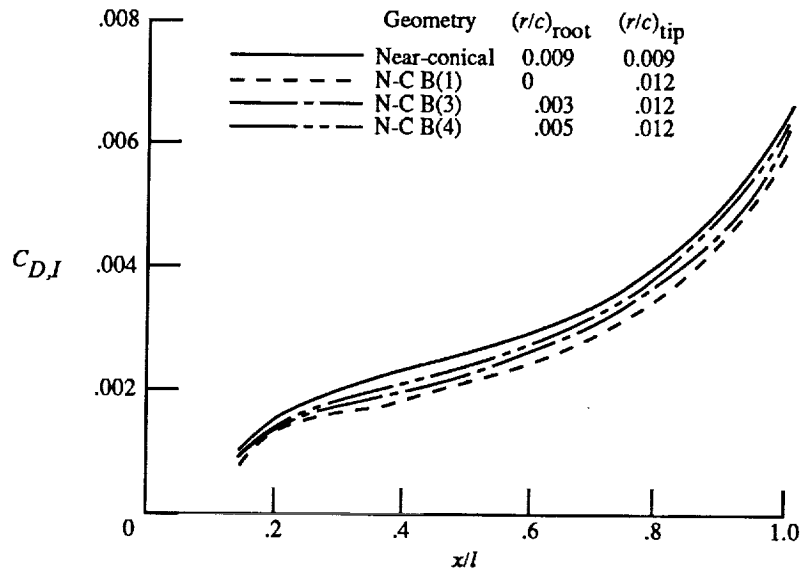
(a) $C_L = 0.1$.
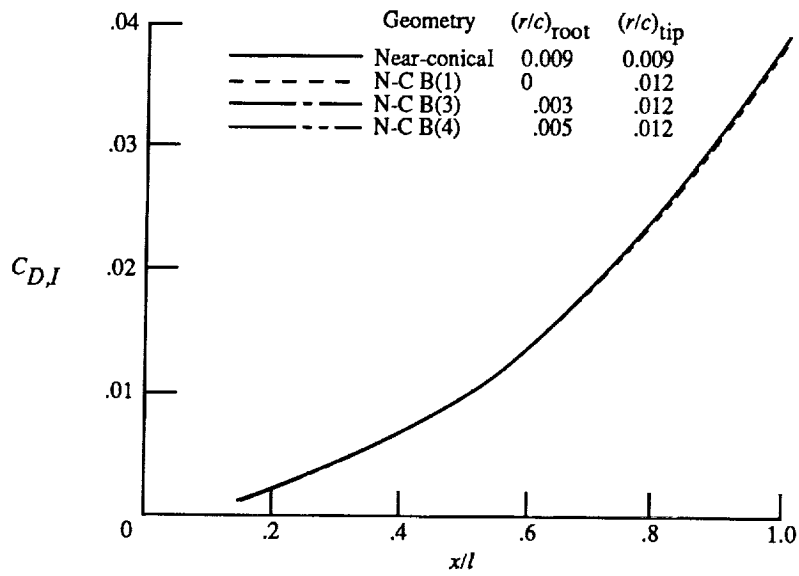
(b) $C_L = 0.3$.

Figure 8. Full-potential predicted drag buildup for variations in leading-edge bluntness for $M = 1.62$ and $C_L = 0.1$ and 0.3.

(a) Near-conical wing.

(b) N-C B(1) wing.
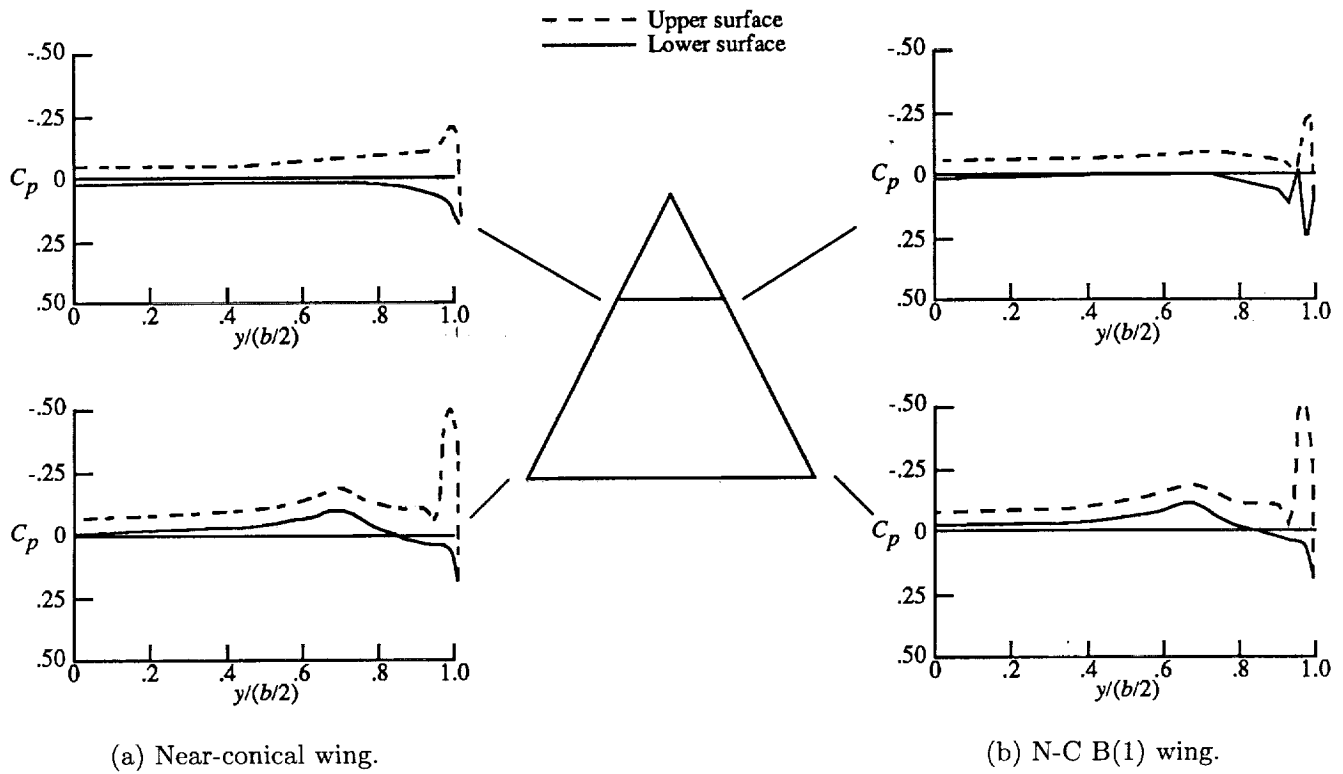
Figure 9. Full-potential predicted surface pressure distributions for near-conical wing and near-conical wing with leading-edge bluntness variation from 0 to 0.012c at $x/l = 0.4$ and 1.0 for $M = 1.62$ and $C_L = 0.1$.
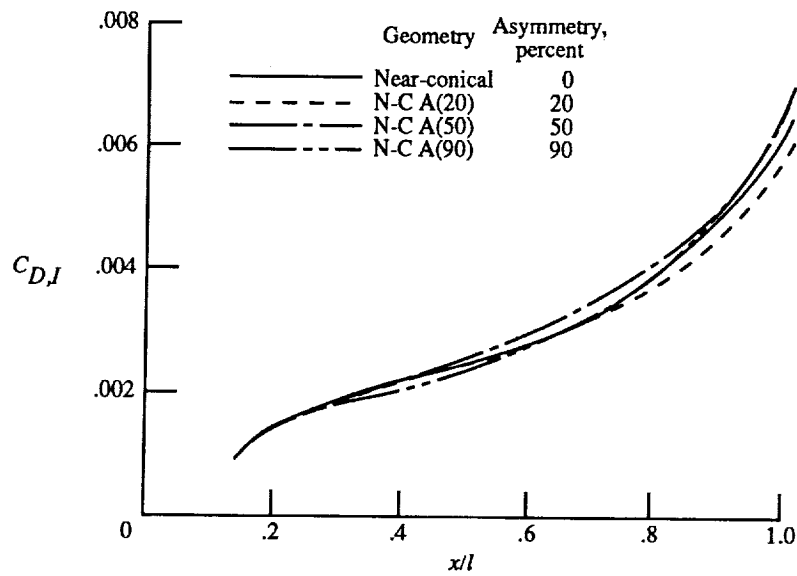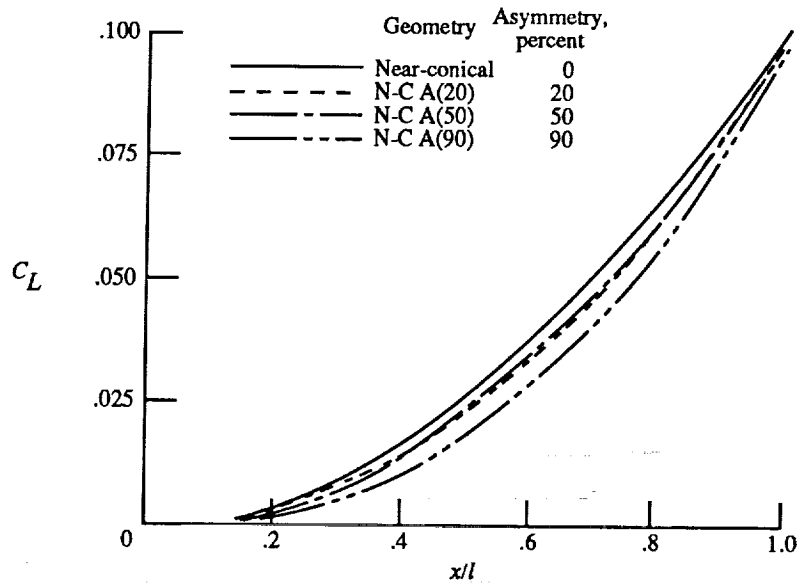
Figure 10. Full-potential predicted lift and drag buildup for variations in wing asymmetry for $M = 1.62$ and $C_L = 0.1$.
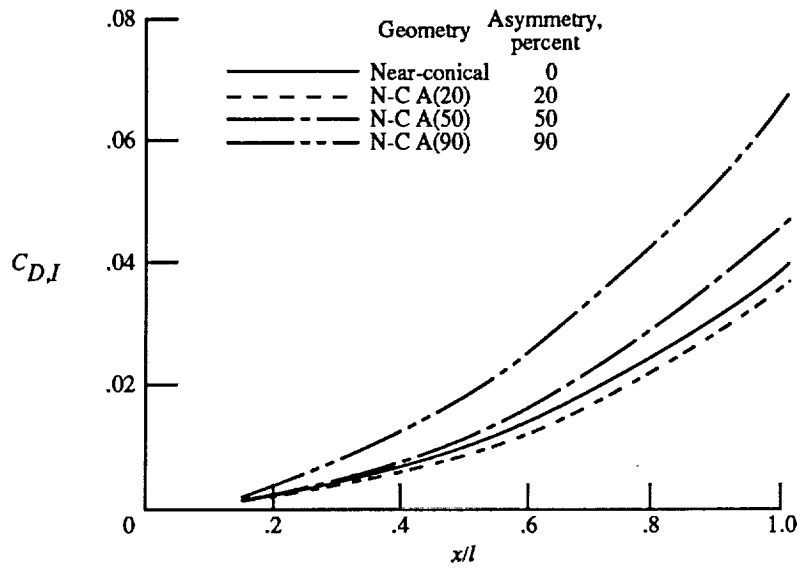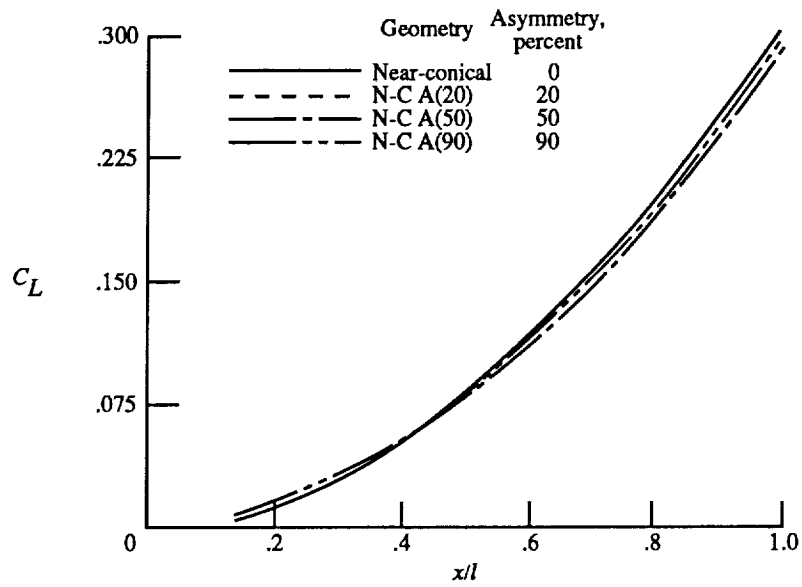
Figure 11. Full-potential predicted lift and drag buildup for variations in wing asymmetry for $M = 1.62$ and $C_L = 0.3$.

(a) Near-conical wing.

(b) N-C A(90) wing and shearing.
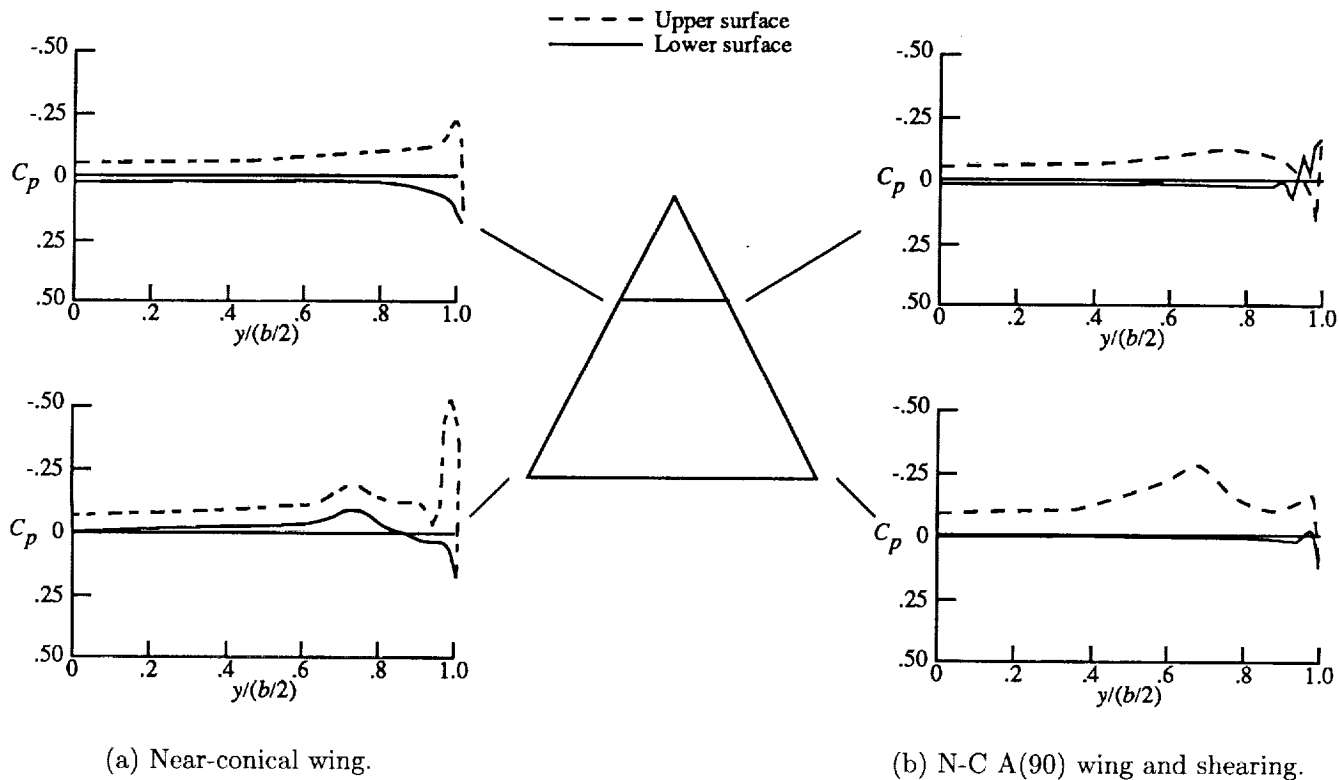
Figure 12. Full-potential predicted surface pressure distributions for near-conical wing and near-conical wing with 90-percent asymmetry and shearing at $x/l = 0.4$ and 1.0 for $M = 1.62$ and $C_L = 0.1$.
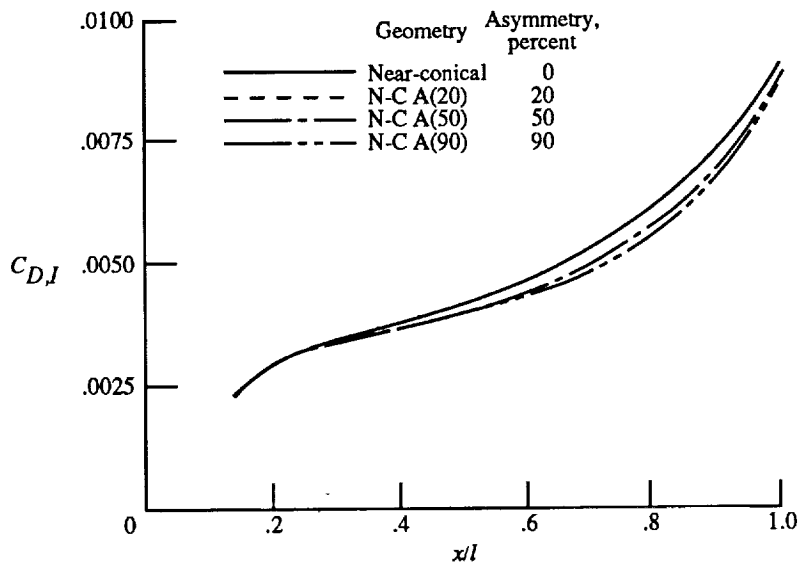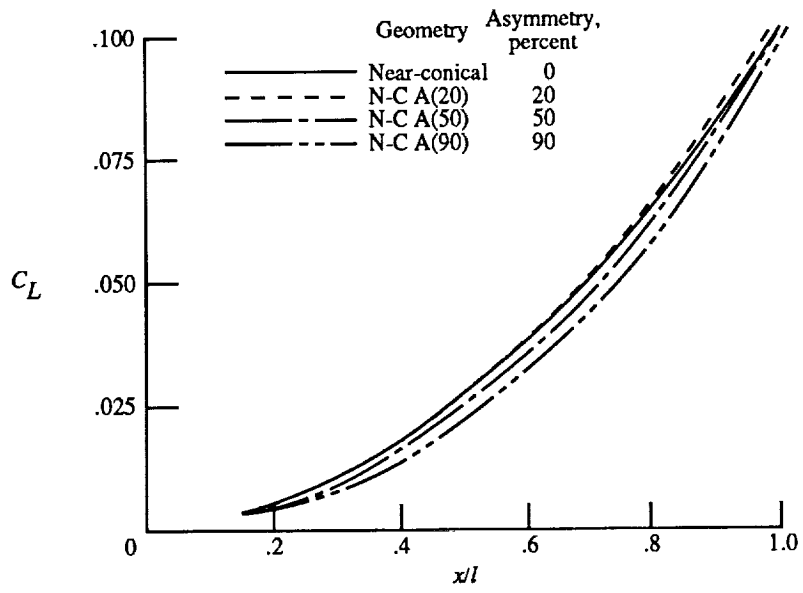
Figure 13. Euler-predicted lift and drag buildup for wing asymmetry variations for $M = 1.62$ and $C_L = 0.1$.
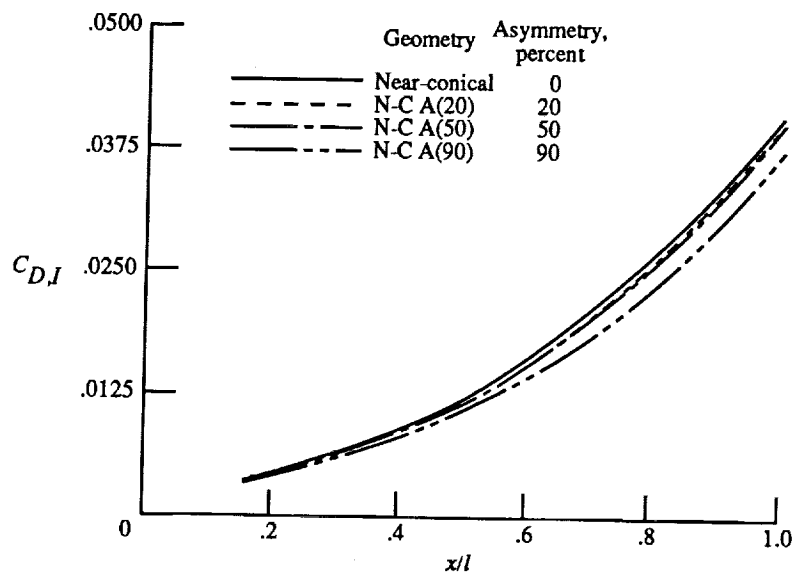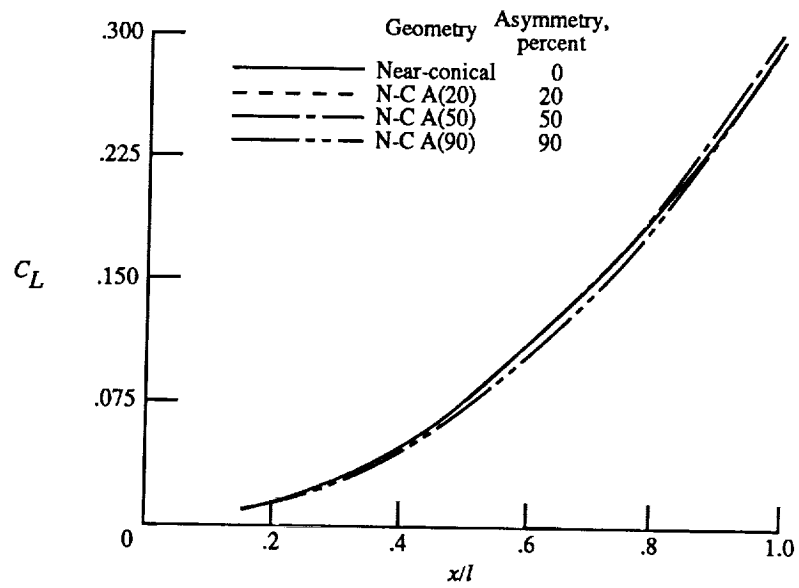
Figure 14. Euler-predicted lift and drag buildup for wing asymmetry variations for $M = 1.62$ and $C_L = 0.3$.

Streamwise cuts

Spanwise cuts

Baseline

Near-conical

N-C B(1)

N-C T(3)

N-C A(90)
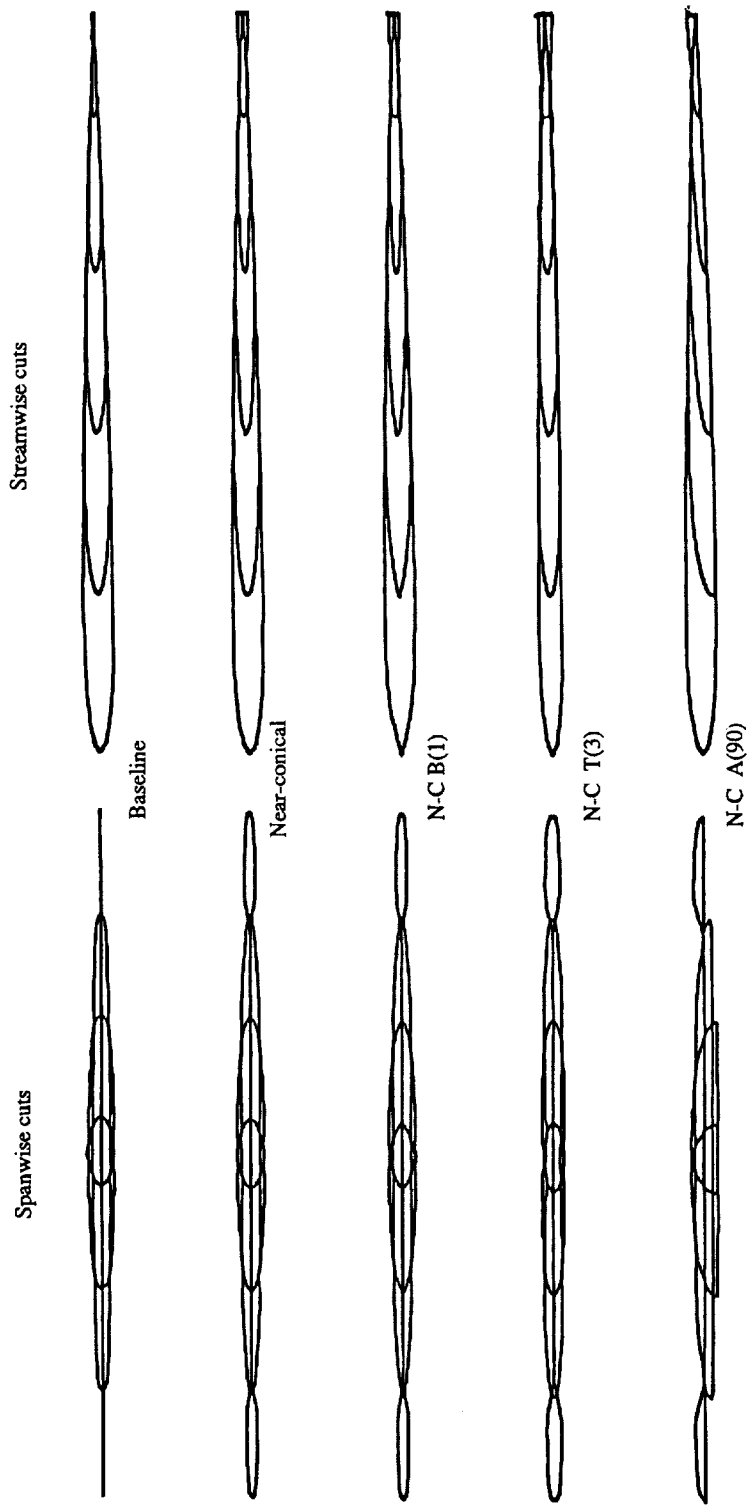
Figure 15. Details of spanwise and streamwise cuts of candidate wing geometries.

27
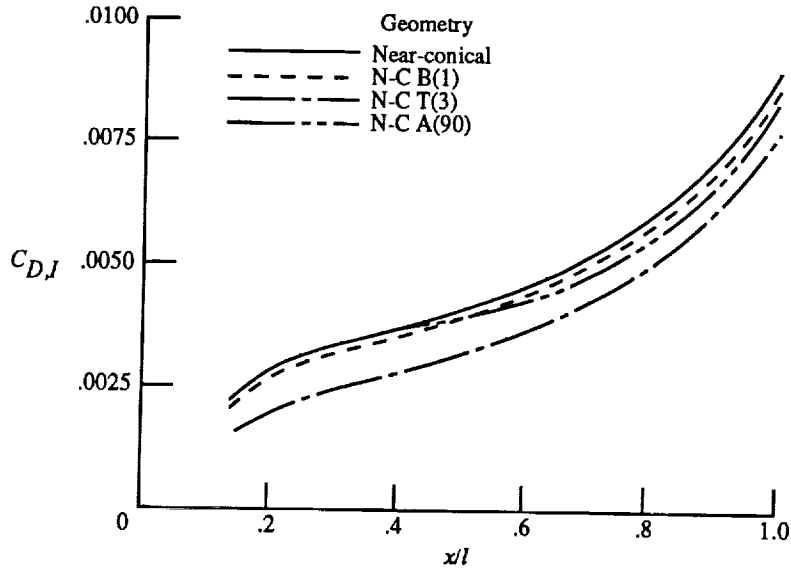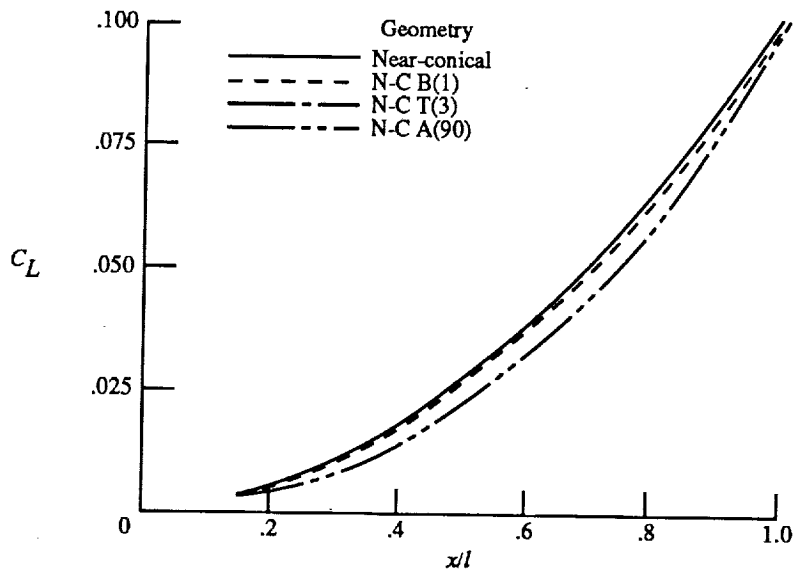
Figure 16. Euler-predicted lift and drag buildup for near-conical wing and near-conical wing with optimum bluntness, thickness, and asymmetry variations for $M = 1.62$ and $C_L = 0.1$.
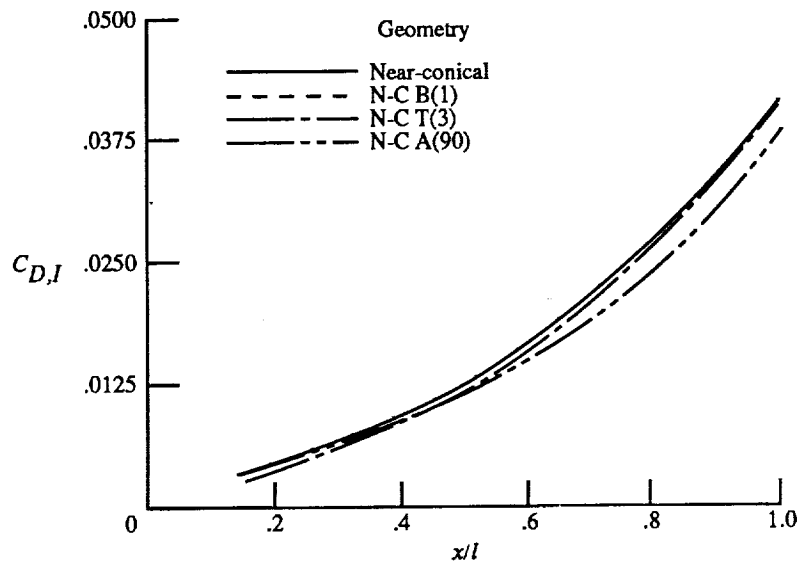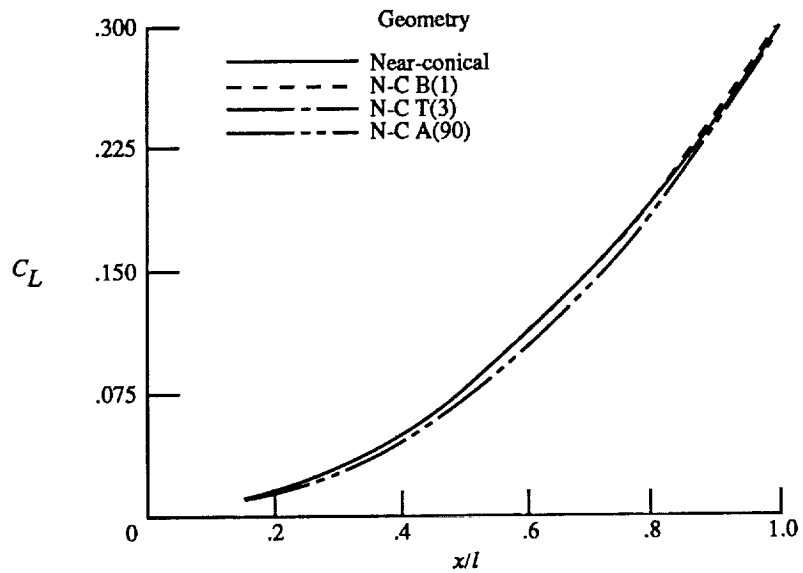
Figure 17. Euler-predicted lift and drag buildup for near-conical wing and near-conical wing with optimum bluntness, thickness, and asymmetry variations for $M = 1.62$ and $C_L = 0.3$.
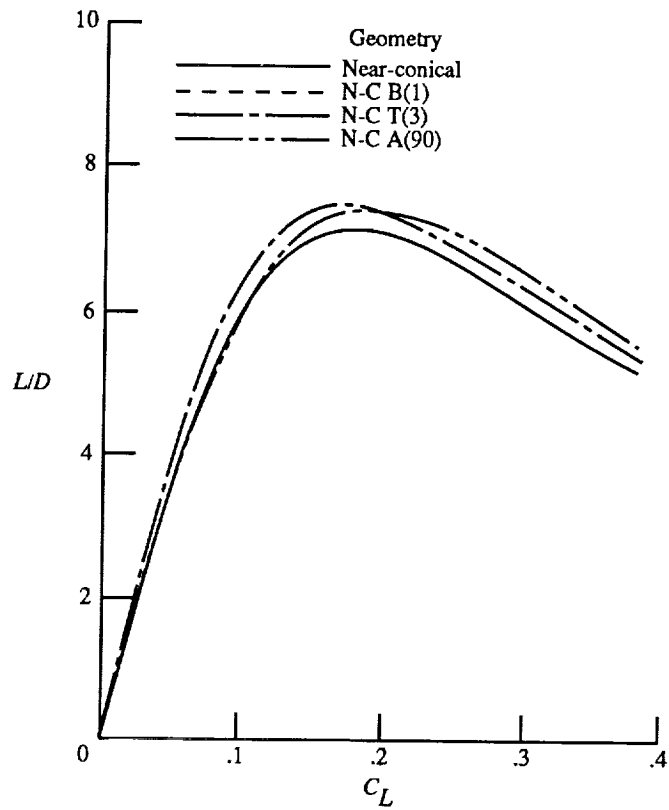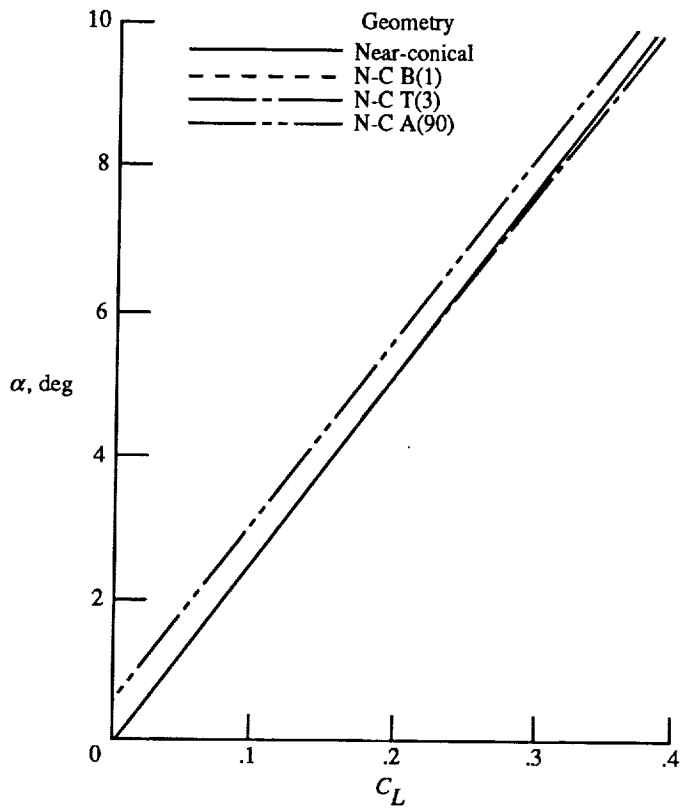
Figure 18. Euler-predicted lift and drag characteristics for near-conical wing and near-conical wing with optimum bluntness, thickness, and asymmetry variations for $M = 1.62$.

Streamwise cuts

Baseline

Near-conical

Natural flow
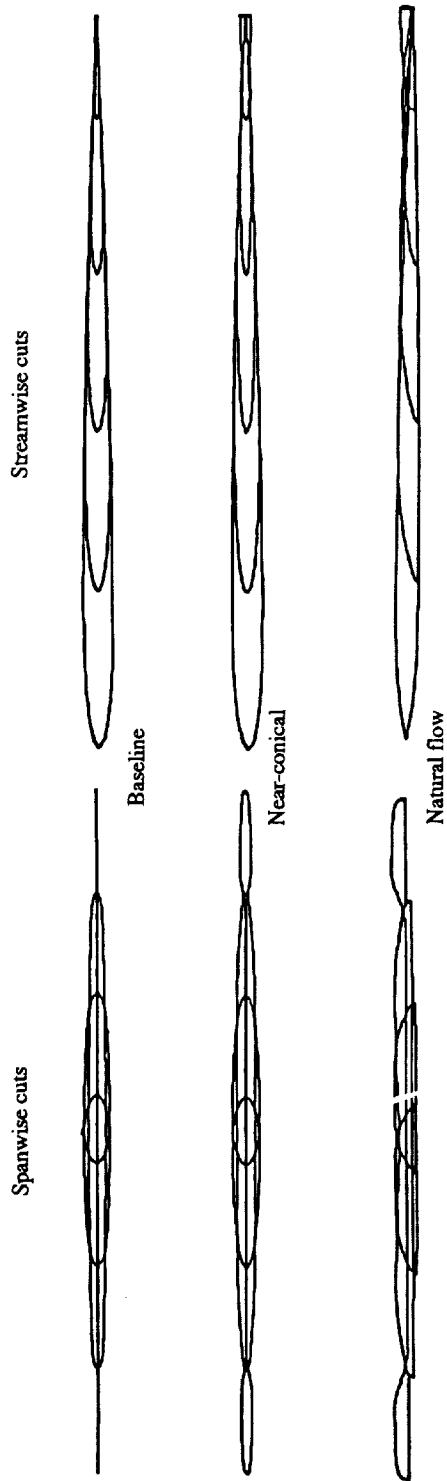
Spanwise cuts

(a) Spanwise and streamwise cuts.

Figure 19. Details of the baseline standard, baseline near-conical, and natural flow wings.

Upper surface
Lower surface

Near-conical

Natural flow
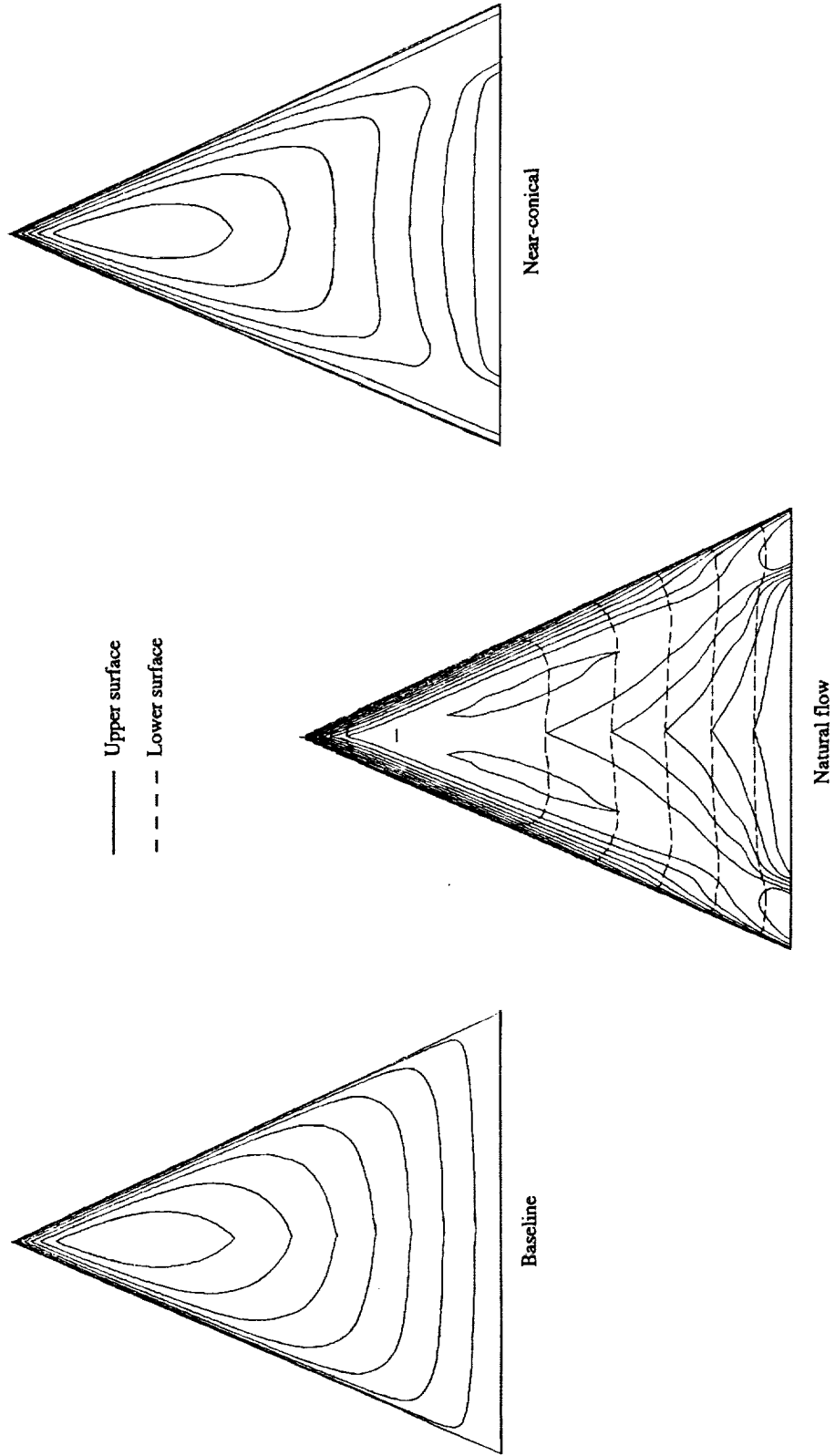
Baseline

(b) Elevation cuts.

Figure 19. Concluded.
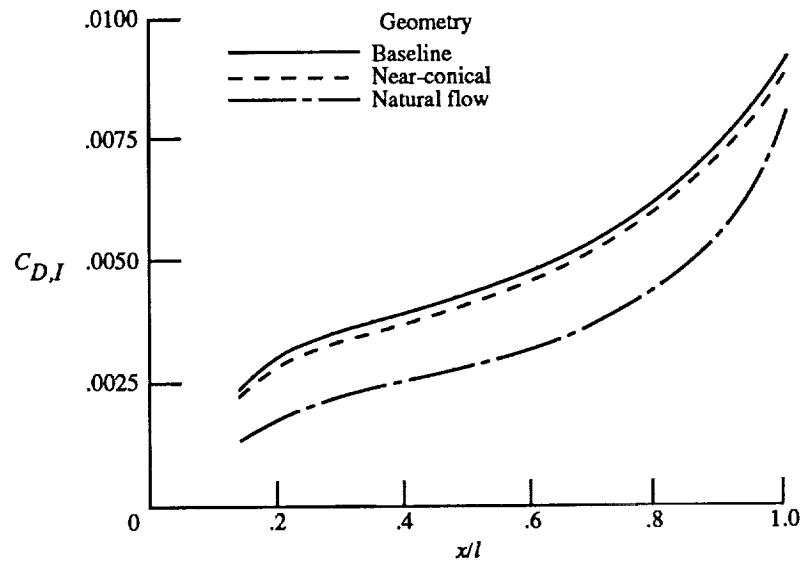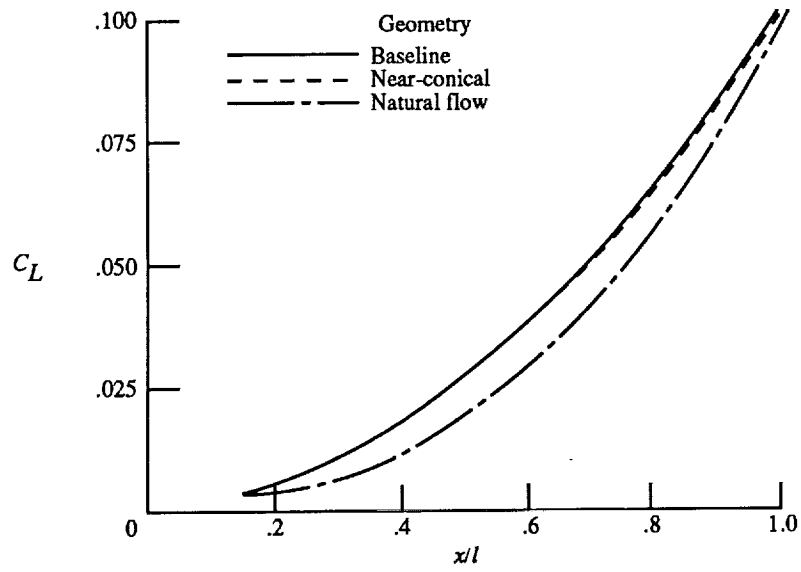
Figure 20. Euler-predicted lift and drag buildup for baseline standard, baseline near-conical, and natural flow wings for $M = 1.62$ and $C_L = 0.1$.
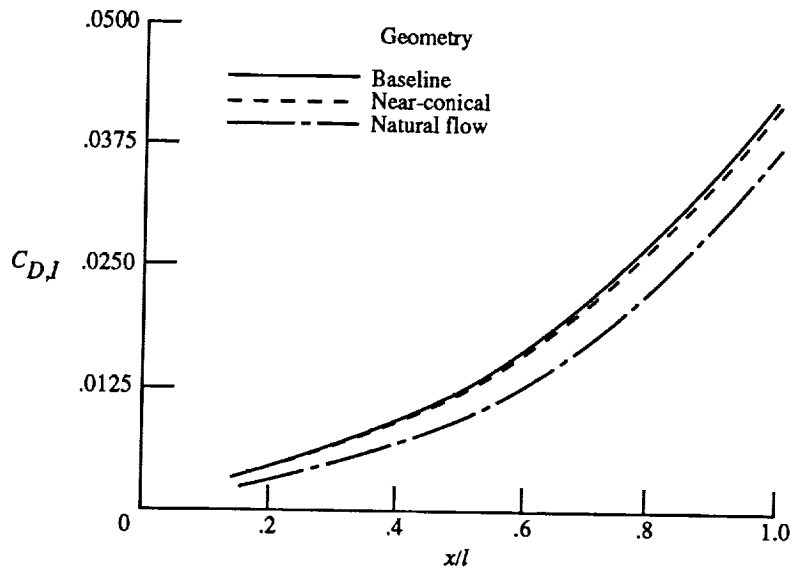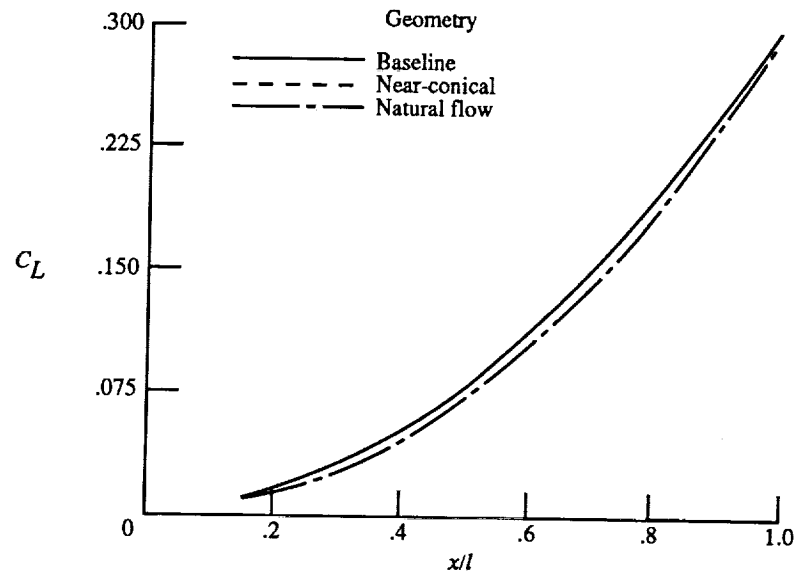
Figure 21. Euler-predicted lift and drag buildup for baseline standard, baseline near-conical, and natural flow wings for $M = 1.62$ and $C_L = 0.3$.
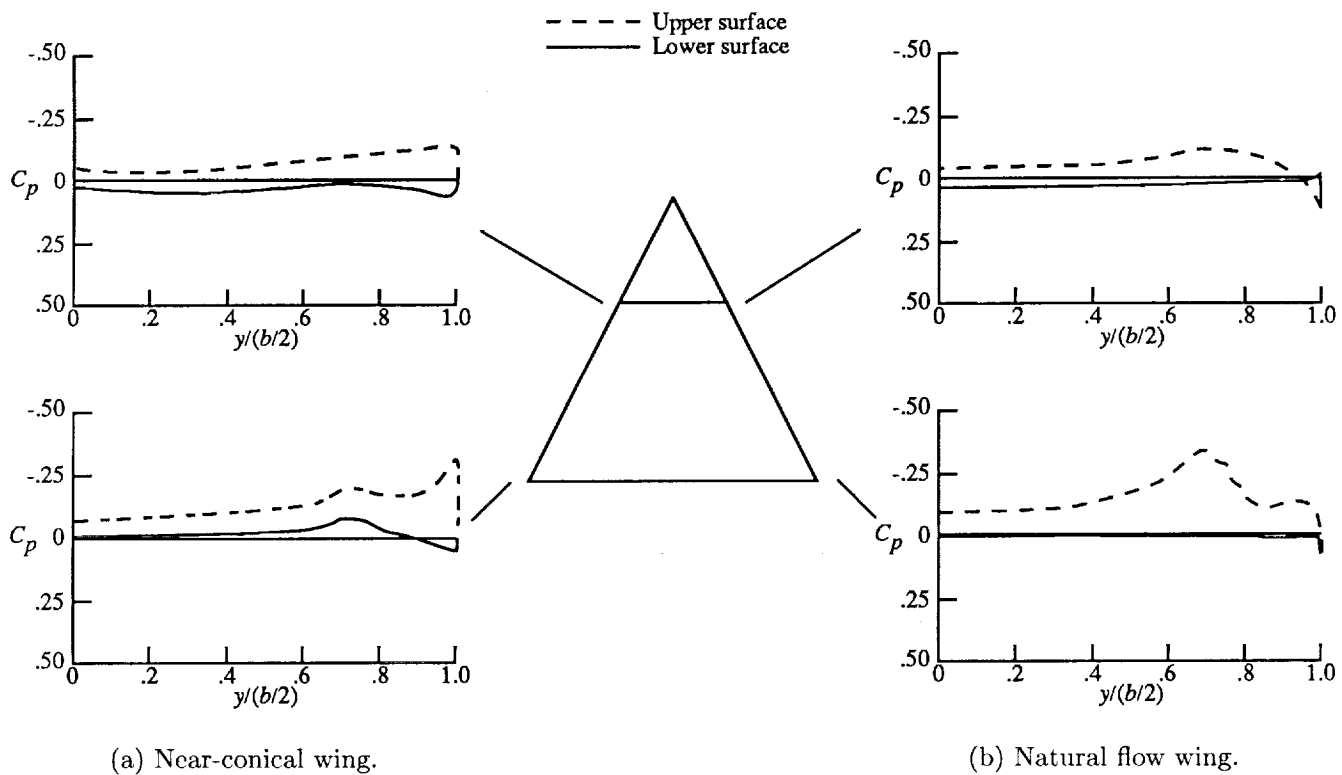
Figure 22. Euler-predicted surface pressure distribution for near-conical wing and natural flow wing (i.e., near-conical wing with optimum bluntness, thickness, and asymmetry variations) at $x/l = 0.4$ and 1.0 for $M = 1.62$ and $C_L = 0.1$.
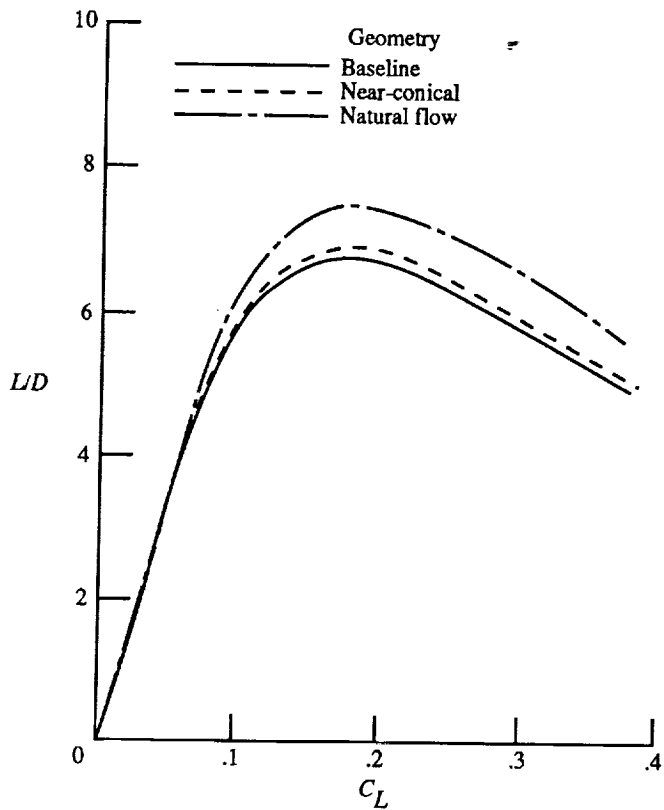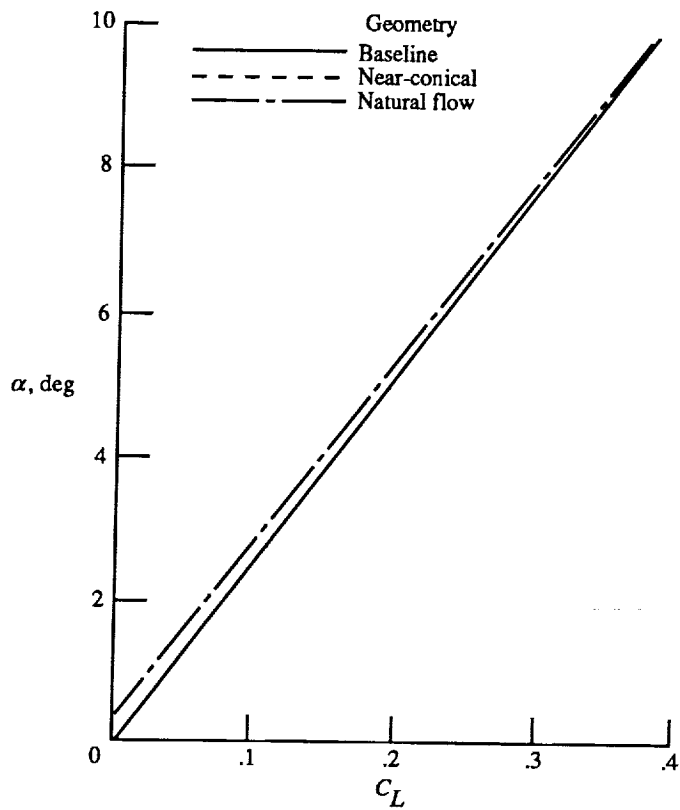
Figure 23. Euler-predicted lift and drag characteristics for baseline standard, baseline near-conical, and natural flow wings for $M = 1.62$.
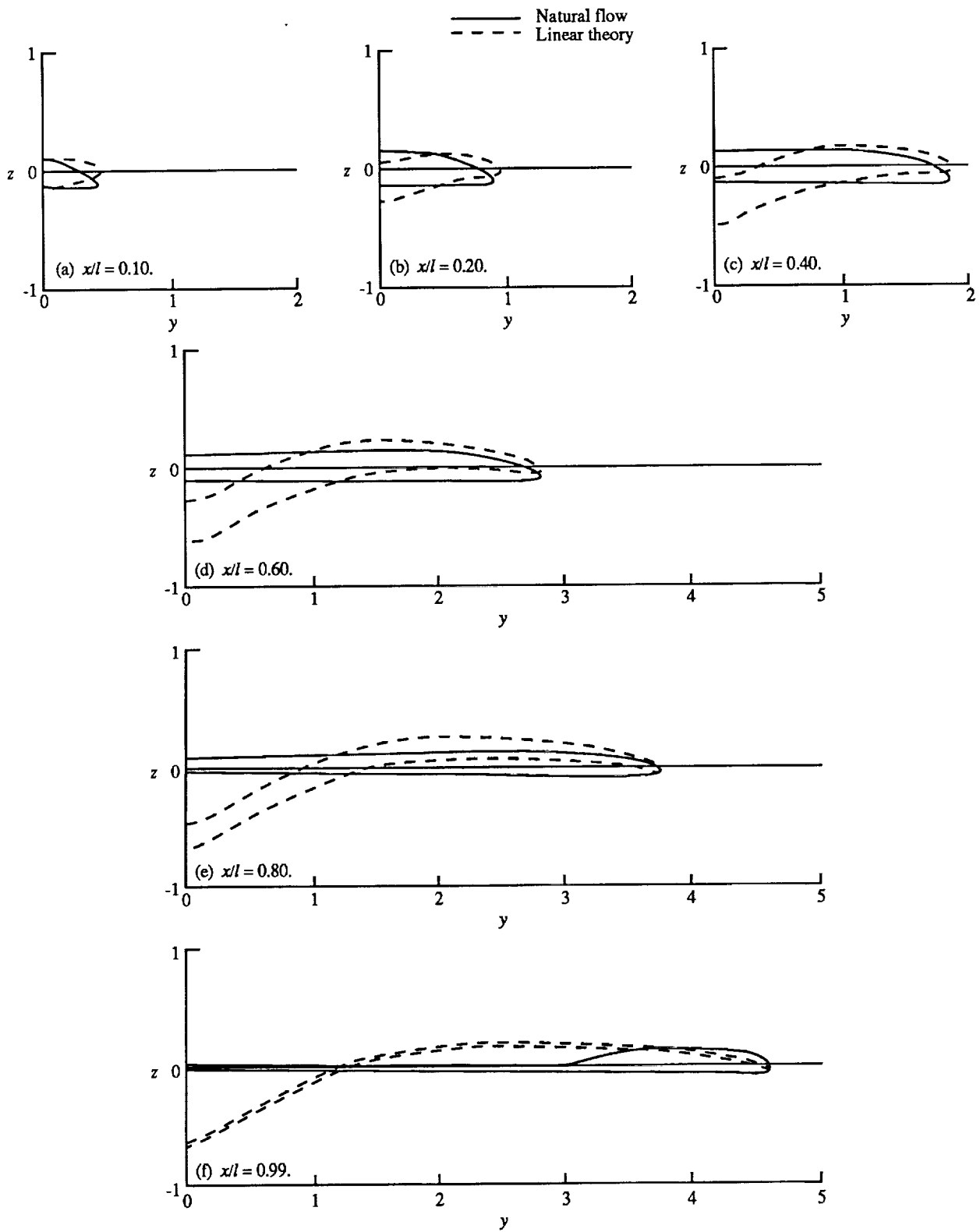
Figure 24. Spanwise cuts of natural flow wing and linear-theory cambered wing. Design $C_L = 0.16$.
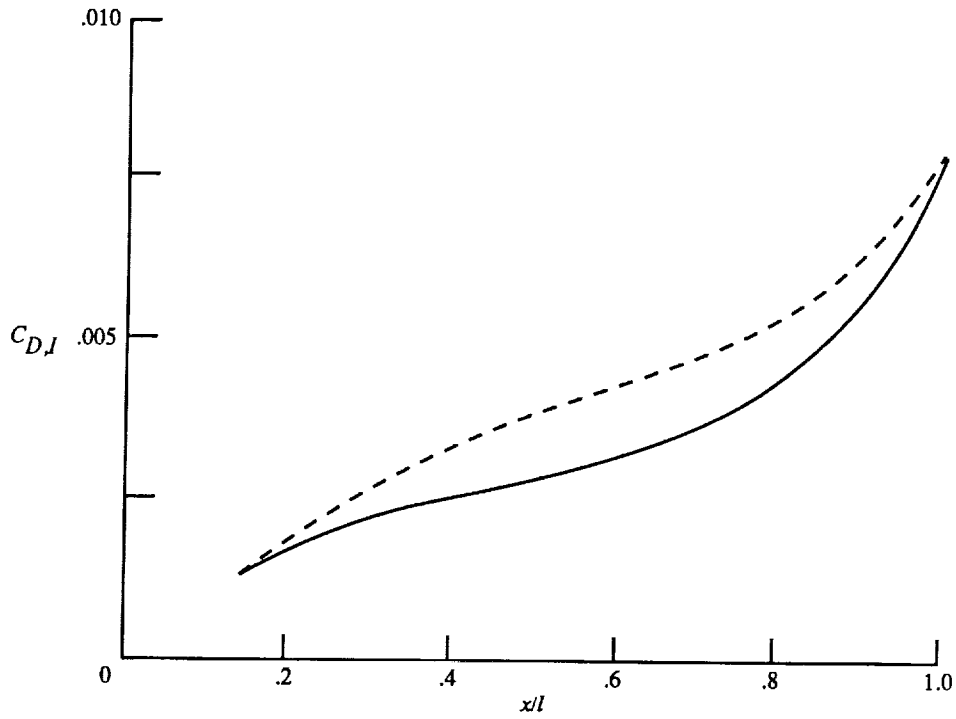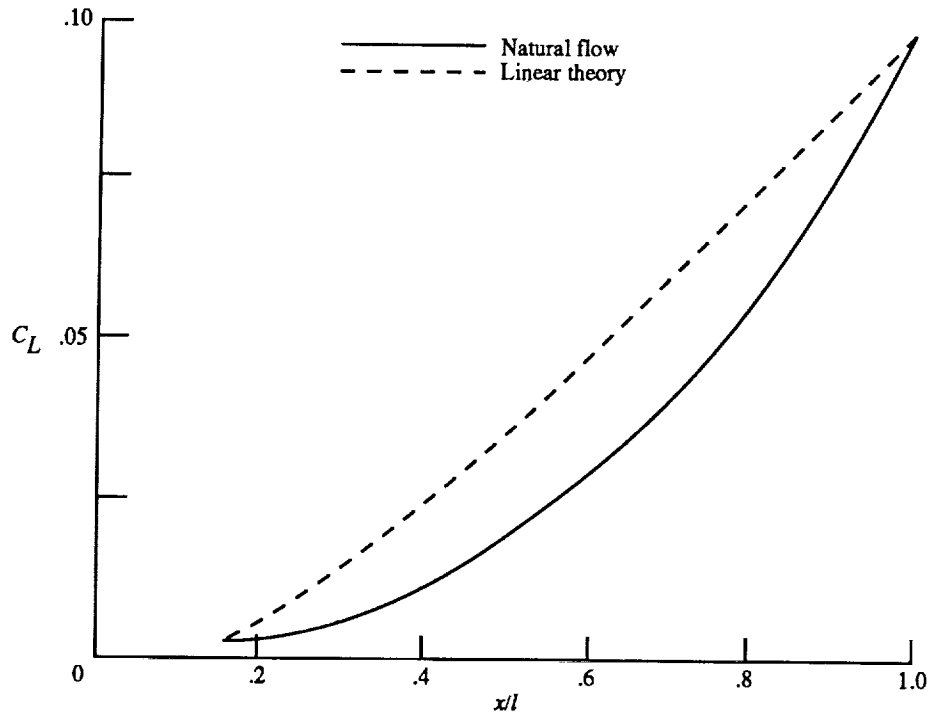
Figure 25. Euler-predicted lift and drag buildup for natural flow wing and linear-theory cambered wing for $M = 1.62$ and $C_L = 0.1$.
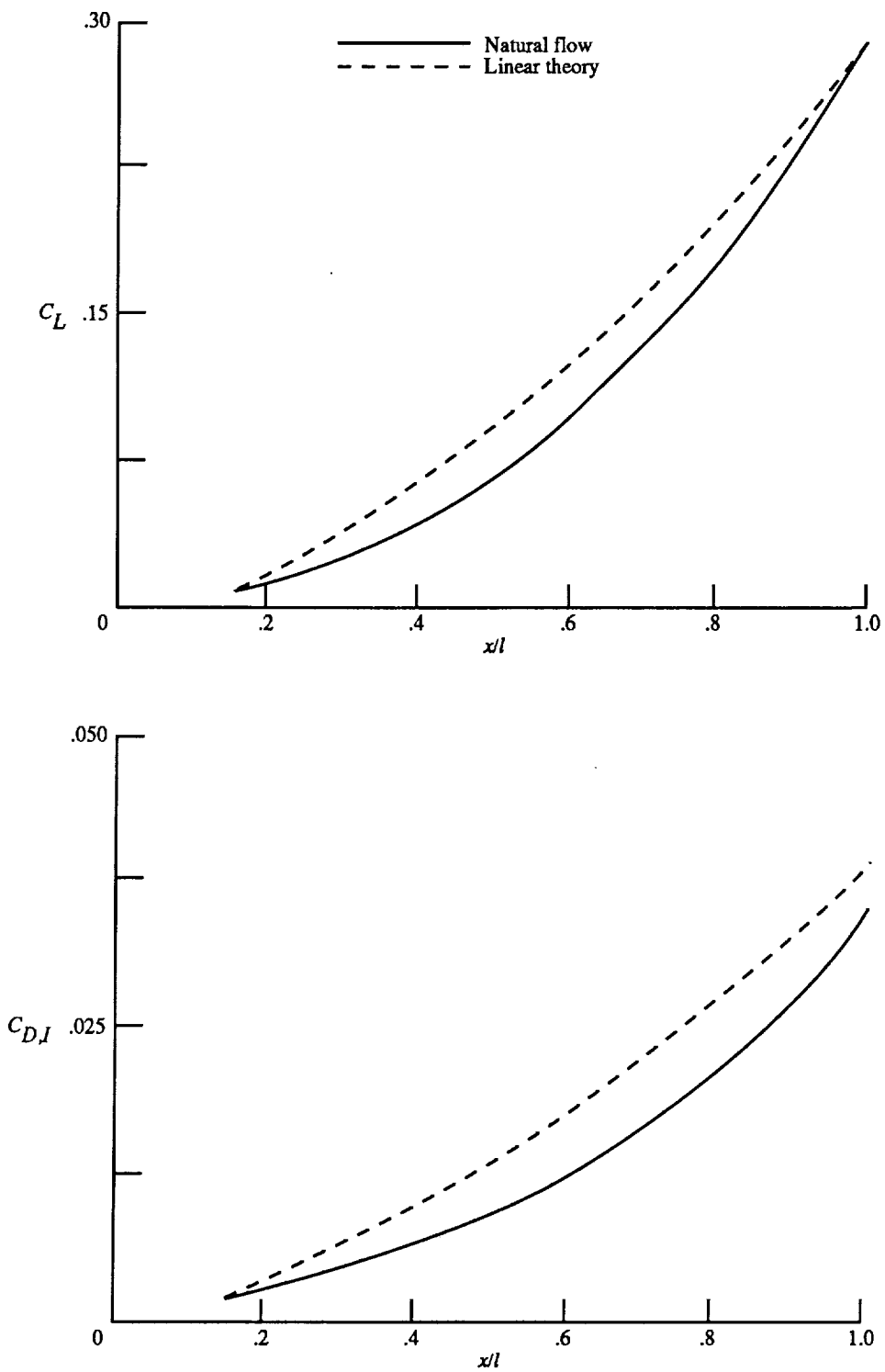
Figure 26. Euler-predicted lift and drag buildup for natural flow wing and linear-theory cambered wing for $M = 1.62$ and $C_L = 0.3$.
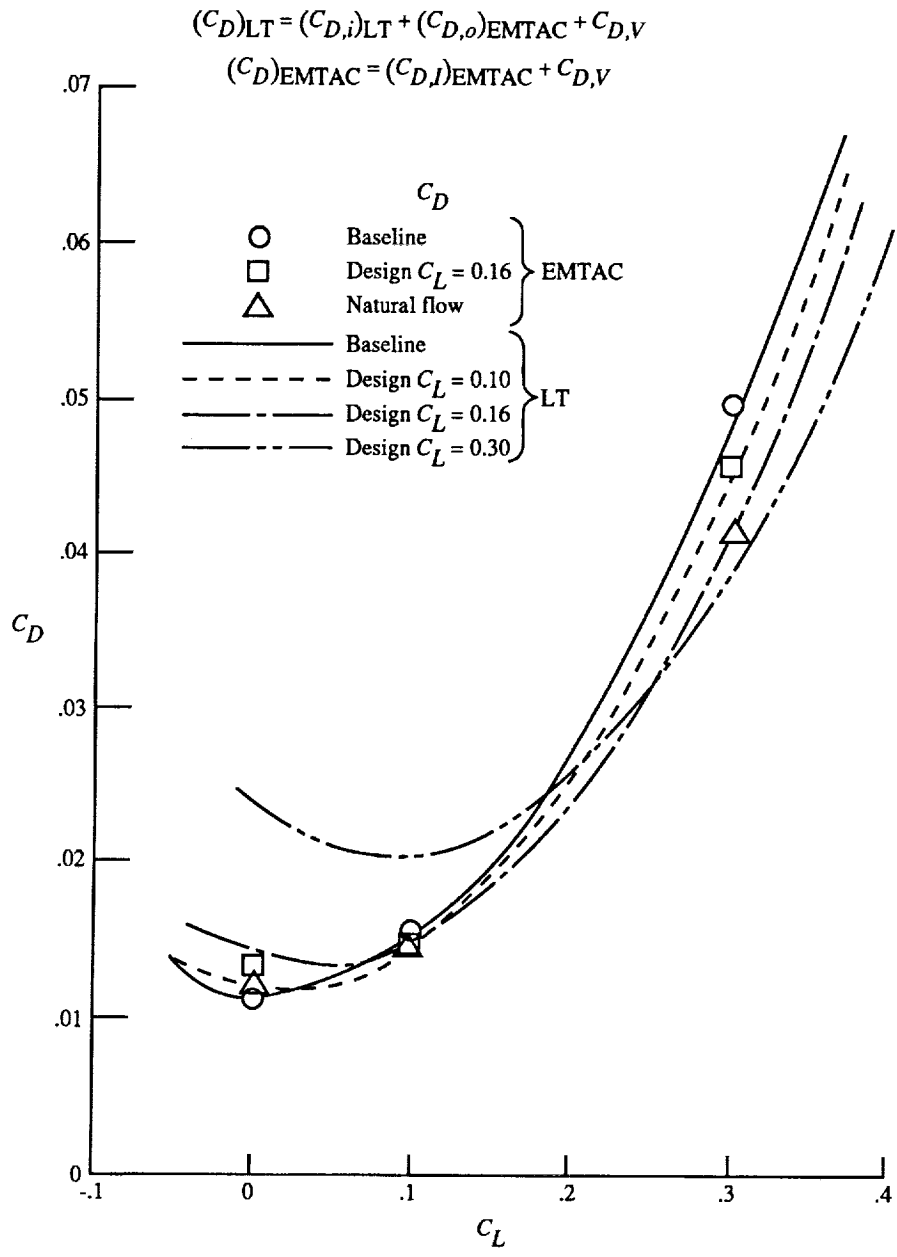
Figure 27. Linear-theory and Euler-predicted drag characteristics for uncambered standard wing, linear-theory cambered wing, and natural flow wing at $M = 1.62$.

REPORT DOCUMENTATION PAGE

1. AGENCY USE ONLY*(Leave blank)*	2. REPORT DATE May 1992	3. REPORT TYPE AND DATES COVERED Technical Paper	

4. TITLE AND SUBTITLE
The Natural Flow Wing-Design Concept

5. FUNDING NUMBERS
WU 505-61-71-01

6. AUTHOR(S)
Richard M. Wood and Steven X. S. Bauer

7. PERFORMING ORGANIZATION NAME(S) AND ADDRESS(ES)
NASA Langley Research Center
Hampton, VA 23665-5225

8. PERFORMING ORGANIZATION REPORT NUMBER
L-16837

9. SPONSORING/MONITORING AGENCY NAME(S) AND ADDRESS(ES)
National Aeronautics and Space Administration
Washington, DC 20546-0001

10. SPONSORING/MONITORING AGENCY REPORT NUMBER
NASA TP-3193

11. SUPPLEMENTARY NOTES

12a. DISTRIBUTION/AVAILABILITY STATEMENT

Unclassified–Unlimited

Subject Category 02

12b. DISTRIBUTION CODE

13. ABSTRACT *(Maximum 200 words)*
A wing-design study has been conducted on a 65° swept leading-edge delta wing in which the wing geometry was modified to take advantage of the naturally occurring flow that forms over a slender wing in a supersonic flow field. Three-dimensional nonlinear analysis methods were used in the study which was divided into three parts—preliminary design, initial design, and final design. In the preliminary design, the wing planform, the design conditions, and the near-conical wing-design concept were derived, and a baseline standard wing (conventional airfoil distribution) and a baseline near-conical wing were chosen. During the initial analysis, a full-potential flow solver was employed to determine the aerodynamic characteristics of the baseline standard delta wing and to investigate modifications of the airfoil thickness, leading-edge radius, airfoil maximum-thickness position, and wing upper to lower surface asymmetry on the baseline near-conical wing. The final design employed an Euler solver to analyze the best wing configurations found in the initial design and to extend the study of wing asymmetry to develop a more refined wing. Benefits resulting from each modification are discussed, and a final "natural flow" wing geometry has been designed that provides an improvement in aerodynamic performance compared with that of a baseline conventional uncambered wing, linear-theory cambered wing, and near-conical wing.

14. SUBJECT TERMS Supersonic; Wing design; Computational fluid dynamics; Drag reduction	15. NUMBER OF PAGES 43
	16. PRICE CODE A03

17. SECURITY CLASSIFICATION OF REPORT Unclassified	18. SECURITY CLASSIFICATION OF THIS PAGE Unclassified	19. SECURITY CLASSIFICATION OF ABSTRACT	20. LIMITATION OF ABSTRACT